



Published in final edited form as:

*Dalton Trans.* 2015 April 21; 44(15): 6809–6824. doi:10.1039/c5dt00257e.

## Ni/Ti layered double hydroxide: synthesis, characterization and application as a photocatalyst for visible light degradation of aqueous methylene blue†

Priyadarshi Roy Chowdhury and Krishna G. Bhattacharyya

Department of Chemistry, Gauhati University, Guwahati 781014, Assam, India

### Abstract

Visible light responsive 2 : 1 Ni/Ti layered double hydroxide (LDH) was synthesized by a single step hydrothermal route using commercially available  $\text{Ni}(\text{NO}_3)_2 \cdot 6\text{H}_2\text{O}$ ,  $\text{TiCl}_4$  and urea. The material exhibited significant absorption in the visible range with a very narrow band gap (2.68 eV). This could be attributed to structural defects as confirmed by diffuse reflectance spectroscopy (DRS), photoluminescence (PL), X-ray diffraction (XRD) and X-ray photoelectron spectroscopy (XPS) measurements. FT-IR, TGA, DTA, DSC, HR-TEM and SEM-EDX measurements yielded information about structural aspects, thermal stability and surface morphology. Surface and pore characteristics of the material were obtained from the BET isotherm for  $\text{N}_2$  adsorption at 77 K. Zeta potential measurements were used to characterize the electrical properties of the surface while XPS revealed changes in surface states and oxygen deficiencies. The material was found to be an excellent photocatalyst for the degradation of aqueous methylene blue in visible light. The photocatalytic properties of the material were explained on the basis of the narrow band gap, the high surface area and the presence of surface defects. The photocatalytic activity improved in alkaline media [pH 11.0, catalyst load 15 mg in 200 ml dye solution, dye concentration  $1 \times 10^{-6}$  M (= 0.3198 mg  $\text{L}^{-1}$ )] due to the electrostatic attractions between the dye cations and the negative charges on the Ni/Ti LDH surface. The catalytic activity was found to be higher than the common commercial catalysts like ZnO, ZnS, NiO,  $\text{TiO}_2$  and Degussa P25. The catalytic activity was retained even after five methylene blue degradation cycles, demonstrating that the LDH could be an important addition to the field of wastewater treatment.

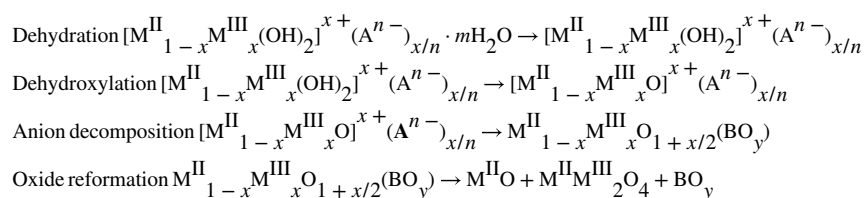
### 1. Introduction

Layered double hydroxides (LDHs), a class of anionic clays, have attracted considerable interest, mainly because of their unique structure with different metal cations as layer constituents as well as different exchangeable anions in galleries. They are widely used as polymer fillers<sup>1–3</sup> and novel materials with magnetic,<sup>4–6</sup> catalytic, and photochemical functions.<sup>7,8</sup> The variability of layered hydroxides arises from a combination of inorganic hydroxide layers with properties contributed by the host anions intercalated between these layers. Ultrathin nanosheets, prepared by delamination of layered hydroxides, have attracted

†Electronic supplementary information (ESI) available: Schematic crystal structure of LDH, HR-TEM image, adsorption equilibrium, XRD lattice parameters, and DTA and DSC measurements of 2 : 1 Ni/Ti LDH. See DOI: 10.1039/c5dt00257e

Correspondence to: Krishna G. Bhattacharyya.

attention due to an extremely small thickness of the order of 1 nm and a large lateral size of the order of micrometers. Comparatively easy preparation, stability in air, interchangeable anions and incorporable host layers have made the LDH an excellent precursor to develop novel photofunctional materials.<sup>9</sup> The general formula of these materials is  $[M^{II}_{1-x}M^{III}_x(OH)_2]^{x+}(A^{n-})_{x/n} \cdot yH_2O$ , where  $M^{II}$  and  $M^{III}$  represent divalent and trivalent cations, respectively, and  $A^{n-}$  is the charge balancing anion. The surface charge can be tuned by varying the ratio of  $M^{II}/M^{III}$  and could be compensated by interlayer anions and water molecules.<sup>10</sup> The structural characteristics and the compositional variability of the LDHs have potential applications in areas such as catalysts, catalyst supports and nanocomposites. The LDH could be readily transformed to the corresponding mixed oxide by heating to a certain temperature, which typically involves dehydration, dehydroxylation, decomposition of anions and oxide segregation in series or in overlapping style as shown below:



where  $M^{II}O$  is an oxide with the rock salt phase,  $M^{II}M^{III}_2O_4$  is a mixed oxide with the spinel phase, and  $BO_y$  denotes the species of decomposed anions. The decomposition processes have their use in designing oxide and oxide-supported catalysts. Specifically, hydrotalcite  $[Mg_3Al(OH)_8] [(CO_3)_{1/2} \cdot 2H_2O]$  undergoes dehydration (100–250 °C), followed by dehydroxylation (350–450 °C) and then decarbonation (420–470 °C) to the rock salt phase  $MgO$  (~450 °C) and mixed oxides (rock salt + spinel) at >700 °C. For LDHs containing oxidizable divalent cations, such as Co(II), Fe(II), Ni(II) and Mn(II), a spontaneous oxidation reaction occurs during heating in air.

Ti containing LDHs have received much attention for their potential application in the removal of toxic substances from industrial wastewater. The present work investigates the role of Ni/Ti LDH in photocatalytic degradation of a common dye, methylene blue, having uses in the printing, textile, and photographic industries.<sup>8,10</sup> The dye is known to cause irritation of skin, eyes and respiratory tract and reportedly possesses carcinogenicity, reproductive and developmental toxicity, neuro- and chronic toxicity towards humans and animals.<sup>11,12</sup> It is therefore important to eliminate this and similar dyes from water so that they do not foul natural water resources.

## 2. Experimental section

### 2.1. Materials

All the chemicals were of analytical grade and were used without any further purification.  $Ni(NO_3)_2 \cdot 6H_2O$ ,  $TiCl_4$ , urea, ZnO, NiO, ZnS, Degussa P25, 2Na-EDTA, *n*-butanol, benzoquinone and methylene blue were purchased from Merck Chemicals, USA. Deionized water (conductivity < 0.15 mS  $cm^{-1}$ ) was used throughout the experiments.

## 2.2. Catalyst synthesis

Ni(NO<sub>3</sub>)<sub>2</sub>·6H<sub>2</sub>O, TiCl<sub>4</sub> as well as urea were used to prepare a hydrotalcite-like material by a co-precipitation method from a homogeneous solution. In a typical synthesis, 11.738 g of Ni- (NO<sub>3</sub>)<sub>2</sub>·6H<sub>2</sub>O, 1.1 ml TiCl<sub>4</sub> and 3.0 g of urea were dissolved in 100 ml deionised water at room temperature and stirred vigorously for 2 h. The resulting mixture was aged in a Teflon lined autoclave at 130 °C for 48 h and the green crystalline product was centrifuged, washed three times with water and dried. This product was denoted as 2 : 1 Ni/Ti-LDH. The synthesis is schematically illustrated in Fig. 1.

## 2.3. Preparation of dye solution

A stock solution of the dye Methylene Blue (MB) (Fig. 2) of concentration  $1.0 \times 10^{-4}$  M (= 31.985 mg L<sup>-1</sup>) was prepared by dissolving an accurately weighed amount in double distilled water. The stock solution was appropriately diluted to obtain experimental dye solutions of concentrations  $1.0 \times 10^{-5}$  (= 3.1985 mg L<sup>-1</sup>) and  $1.0 \times 10^{-6}$  M (= 0.3198 mg L<sup>-1</sup>).

## 2.4. Characterization techniques

Powder X-ray diffraction (XRD) patterns were obtained with a PANalytical X'Pert PRO diffractometer that allowed both reflection and transmission experiments on the same sample. Reflection mode experiments were set up using the conventional Bragg–Brentano geometry. The incident X-ray beam (CuK<sub>α</sub>, 40 kV, 30 mA) passed through a 0.02 rad Soller slit, a 1/8 divergence slit, a 15 mm fixed mask, and a 1/4 anti-scatter slit. The diffracted beam was detected by a PIXcel linear position sensitive detector equipped with a β filter, a 0.02 rad Soller slit, and a 1/8 anti-scatter slit. The XRD patterns were recorded between 5 and 80° (2θ) with a step size of 0.013° and an acquisition time of 500 s per step. The transmission-mode data were collected using an elliptic focusing mirror, a 0.5° divergence slit, a 0.5° anti-scatter slit and a 0.02 rad Soller slit in the primary beam. Fourier Transform Infrared spectroscopy (FT-IR) measurements were carried out with a Shimadzu FT-IR 3000 spectrometer (resolution 4 cm<sup>-1</sup>), the sample was pressed into KBr discs with a weight ratio of sample to KBr of 1 : 100. Thermal analyses (TGA/ DTG, TG/DTA and TG/DSC) were carried out with a Mettler Toledo thermal analyser system from 32 °C to 750 °C under a N<sub>2</sub> atmosphere with a heating rate of 10 °C min<sup>-1</sup>. The specific surface area, pore volume and pore size analyses were performed with a Micromeritics TriStar 3000 V6.08 analyzer using Brunauer–Emmett– Teller (BET) and Barret–Joyner–Halender (BJH) methods. Prior to the measurements, the samples were degassed at 120 °C for 3.0 h. X-ray photoelectron spectroscopy (XPS) analyses were obtained with a PHI Quantum 5800 ESCA instrument, equipped with a micro-focussing monochromated Al K<sub>α</sub> X-ray source. The solid UV– vis diffuse reflectance spectrum was recorded at room temperature with a Hitachi U4100 spectrometer using BaSO<sub>4</sub> background. The morphology and the elemental composition of 2 : 1 Ni/Ti LDH were investigated with a scanning electron microscope (Zeiss Supra 55) at an accelerating voltage of 20 kV, coupled with an energy dispersive X-ray spectrometer (EDX) with an Oxford INCA EDX 300 microanalysis attachment. High resolution transmission electron microscopy (HR-TEM) images were recorded with the help of a Philips TECNAI-20 equipped with a JEOL JEM-2010 high-resolution transmission electron

microscope. The accelerating voltage was 200 kV. The zeta potential was measured using a Malvern Zetasizer Nano ZS instrument at different pH values. Photoluminescence spectra of the Ni/Ti LDH sample were obtained at room temperature on a fluorescence spectrometer (Hitachi F-2500 FL spectrophotometer) with a xenon lamp as the excitation source. The absorption spectra in the photodegradation process were monitored with a Shimadzu 1800 UV-Vis spectrometer.

## 2.5. Photocatalytic reactions

The photocatalytic reactor (Fig. 3) consisted of a stainless steel chamber fitted with a 300 W tungsten lamp (Philips 38941-1; PS 25, Frost-6100) as the visible-light source, equipped with a wavelength filter ( $\lambda > 400$  nm) at the bottom. The degradation experiments of the dye were carried out at 30 °C and the reaction mixture was taken in a double walled beaker with continuous circulation of running water in the outer jacket ensuring constant temperature of the reaction mixture. In all the degradation experiments, the reactants were vigorously stirred for 30 min in the dark to establish an adsorption/desorption equilibrium between the catalyst and the dye, followed by exposure to visible-light irradiation. 10 ml aliquots were taken out at 15 min intervals and centrifuged to remove solid catalyst particles and the centrifugate was analyzed for the unconverted dye using a Shimadzu UV-1800 spectrophotometer at a  $\lambda_{\text{max}}$  of 664 nm. The reaction blank was carried out with the same procedure without adding the catalyst. A set of control reactions with the catalyst was carried out in the dark for 75 min. The effects of pH on the photocatalytic degradation were investigated by varying the pH of the reaction mixture from 5.0 to 11.0 by adding either hydrochloric acid or sodium hydroxide (0.1 M). Catalyst loadings of 5.0, 10.0, 15.0 and 20.0 mg in 200 ml dye solution were used to investigate the effects of the same on methylene blue photo-degradation at pH 11.0 and a dye concentration of  $1.0 \times 10^{-6}$  M (= 0.3198 mg L<sup>-1</sup>). The photocatalytic conversion of the dye was done at three different concentrations of  $1.0 \times 10^{-4}$ ,  $1.0 \times 10^{-5}$  and  $1.0 \times 10^{-6}$  M with a catalyst loading of 15.0 mg and pH 11.0. The performance of the material was compared with that of commercially available pure ZnO, ZnS, NiO and TiO<sub>2</sub> as a photocatalyst (15 mg in 200 ml of dye solution) for methylene blue of concentration  $1.0 \times 10^{-6}$  M (= 0.3198 mg L<sup>-1</sup>) degradation.

## 3. Results and discussion

### 3.1. XRD analysis

The powder X-ray diffraction pattern of the LDH (Fig. 4) revealed a typical layered structure with high crystallinity, similar to those previously reported in the literature for LDH-like materials.<sup>13–15</sup> The diffraction bands are in good agreement with the characteristic hexagonal phase of LDH.<sup>1</sup> The (003), (006), (009) and (100) bands appeared at 13.69°, 27.38°, 41.07° and 31.62° ( $2\theta$ ) respectively. The basal spacing corresponding to  $d_{(003)}$  was 0.763 nm ( $2\theta \approx 13.32^\circ$ ) and that of  $d_{(110)}$  was 0.153 nm ( $2\theta \approx 27.31^\circ$ ). For the frequently occurring carbonate form of LDH, a basal spacing of 0.76 nm has been reported for the reflection at approximately  $2\theta \approx 11.7^\circ$  in the XRD profile.<sup>9</sup> The shift in the basal reflection to a higher  $2\theta$  (13.69°) in Ni/Ti LDHs is likely to be related to the presence of divalent Ni(II) and tetravalent Ti(IV) in the host layers whereas a  $2\theta$  value of 11.7° is normally

reported for the natural and synthetic carbonate hydrotalcites with trivalent and tetravalent cations.<sup>11</sup>

Since 2 : 1 Ni/Ti LDH has been found to have the same basal spacing as that in normal LDHs, it is likely that the planar orientation of anions, mainly carbonate, and water molecules in the interlayer space has remained almost in a similar pattern in the LDH prepared in this work. The addition of TiCl<sub>4</sub> in the aqueous media at room temperature during catalyst synthesis has generated TiO<sub>2</sub> and is evident from the diffraction peaks in the XRD profile of the layered material. The XRD pattern exhibited strong diffraction peaks (110) and (101) at  $2\theta$  values of 27.31° and 37.81° indicating the presence of TiO<sub>2</sub> in the anatase phase in the layered material.<sup>13</sup> The XRD pattern also had peaks at (011), (018), (113) and (1013) which could be indexed to typical LDH materials.<sup>14–18</sup> The narrow and sharp diffraction peaks indicate that the samples have good crystallinity. The contraction in the interlayer distance of 2 : 1 Ni/Ti LDH is possibly related to strong electrostatic interactions between the host layer and the guest carbonate species in the presence of Ti(IV).<sup>10–12</sup> Moreover, reflection at  $2\theta = 22.3^\circ$  could be assigned to the presence of a small amount of NiO<sub>x</sub> impurity. The important XRD characteristics of 2 : 1 Ni/Ti LDH in terms of the lattice parameter,  $a (= 2d_{110})$ , and the interlayer thickness,  $c [= (3d_{003} + 6d_{006} + 9d_{009})/3]$ , are available in S3 and S4 of ESI†.<sup>12,16–18,35</sup>

### 3.2. FT-IR analysis

The FT-IR spectrum recorded at room temperature showed the characteristic frequencies associated with the layered structure of the LDH materials (Fig. 5). All the key bands resemble those exhibited by the hydrotalcite-like phase with CO<sub>3</sub><sup>2-</sup> as the counter anion. An intense broad strong absorption band centered at 3450 cm<sup>-1</sup> is attributed to the stretching vibrations of surface and interlayer water molecules and hydroxyl groups usually observed at lower frequency in the LDH rather than in the OH stretching vibration in free water at 3600 cm<sup>-1</sup>. This is related to the formation of hydrogen bonds of interlayer water with guest anions as well as with hydroxide groups of layers.<sup>1</sup> The broad band at 3141 cm<sup>-1</sup> accompanied by a shoulder at nearly 3023 cm<sup>-1</sup> can be assigned to the hydrogen bonding between water and carbonate in the interlayer. The band at 1605 cm<sup>-1</sup> is assigned to the bending vibration of water molecules.

In most of the hydrotalcites, there are three IR active absorption bands arising from the carbonate anion observed at 1384 cm<sup>-1</sup> ( $\nu_3$ ), 1058 cm<sup>-1</sup> ( $\nu_1$ ) and 745 cm<sup>-1</sup> ( $\nu_2$ ). The band at 1384 cm<sup>-1</sup> is assigned to  $\nu_3$  mode of CO<sub>3</sub><sup>2-</sup> species in the LDH interlayer.<sup>9</sup> The bands at 996 cm<sup>-1</sup> and 826 cm<sup>-1</sup> are associated with metal–oxygen (M–O) and metal–hydroxyl (M–OH) groups in the lattice of LDHs.<sup>17,22</sup> The sharp band at 835 cm<sup>-1</sup> is associated with in-plane quadrant bending.<sup>8</sup> Another peak at 1109 cm<sup>-1</sup> is associated with C–O single bond stretching vibrations. The band at approximately 745 cm<sup>-1</sup> is attributed to  $\nu_2$  mode of the CO<sub>3</sub><sup>2-</sup> species.<sup>12,18–22</sup> The presence of all these bands, combined with XRD results, confirms successful incorporation of CO<sub>3</sub><sup>2-</sup> and H<sub>2</sub>O molecules into the interlayer gallery of the LDH prepared by the hydrothermal route.

†Electronic supplementary information (ESI) available: Schematic crystal structure of LDH, HR-TEM image, adsorption equilibrium, XRD lattice parameters, and DTA and DSC measurements of 2 : 1 Ni/Ti LDH. See DOI: 10.1039/c5dt00257e

### 3.3. Thermogravimetric analysis

The thermogravimetric analysis (TGA) of Ni/Ti LDH (Fig. 6) is comparable with previous data obtained for LDH-like materials.<sup>3</sup> The thermal stability of the synthesized 2 : 1 Ni/Ti-LDH could be represented in terms of three degradation steps. The weight loss observed between 70 and 130 °C with a broad peak at 91 °C in the DTG curve was due to the removal of physically adsorbed and interlayer water constituting 14.01% by weight of the material. The second weight loss was observed between 260 and 300 °C with a sharp peak at 298 °C accounting for 14.8% by weight and was due to a concomitant dehydration of the brucite-like layers. This was followed by a larger weight loss of 21.5% observed between 300 and 425 °C, associated with a broad peak at 372 °C, which was likely to have occurred as a result of decomposition of  $\text{CO}_3^{2-}$  in the interlayer positions.<sup>17,18</sup> The material did not suffer any significant weight loss above 500 °C indicating that the presence and decomposition of residual carbonaceous compounds were almost zero. The thermal analyses performed with DTA and DSC also indicate the validity of the TGA results. (Details of the analyses are available in S5 and S6 of ESI.<sup>†</sup>) Thus weight loss measurements are in agreement with the presence of  $\text{H}_2\text{O}$  molecules and  $\text{CO}_3^{2-}$  anions in the interlayer gallery of LDH as found from XRD and FT-IR measurements.

### 3.4. HR-TEM analysis

The morphology of the synthesized Ni/Ti LDH was investigated by cross-sectional high-resolution transmission electron microscopy (HR-TEM) indicated in Fig. 7(A, B, C). Fig. 7A reveals non-uniform, round-edged hexagonal platelets stacked one over the other in good agreement with the SEM observations (Fig. 7D). The selected area electron diffraction (SAED) pattern (Fig. 7B) indicated bright spots revealing the crystallinity of the material, in agreement with the XRD results. A well-ordered layered structure is observed from Fig. 7C. The interlayer distance between the periodic lattice fringes from the (110) plane of 2 : 1 Ni/Ti-LDH (inset plot, Fig. 7C) was approximately 0.153 nm, in good agreement with the  $d_{(110)}$  value of 0.153 nm, determined from the X-ray diffraction studies (S3, ESI<sup>†</sup>).

### 3.5. SEM/EDX analysis

The SEM image of the Ni/Ti LDH (Fig. 7D) reveals a microspheric morphology in good agreement with the regular hexagonal shaped particles stacked on top of each other, a characteristic of the lamellar phases of LDH compounds. The as-synthesized Ni/Ti LDH is composed of a large number of platelets about 12 nm in width which could be evidence of subsequent crystallization of layered double hydroxide incorporated with  $\text{CO}_3^{2-}$  and  $\text{H}_2\text{O}$  molecules into the interlayer.<sup>19–24</sup> In this case, the composite material exhibited non-uniform, round edged, hexagonal plate-like particles with pores of different sizes. Very likely, the presence of  $\text{CO}_3^{2-}$  in the interlamellar space has produced a change of the superficial interaction between particles that influenced the aggregation of the particles forming a 3D architecture, giving rise to pores of different sizes. In a slow precipitation process, hydrotalcite-like structures give hexagonal plates that display rounding of the edges upon intercalation.<sup>1,18,25</sup> Most importantly, these pores can serve as the transportation paths of various species.

In order to estimate the elemental composition of Ni/Ti LDH, the elemental analysis was done using energy-dispersive X-ray spectroscopy (EDX) (Fig. 8). The EDX analysis shows the presence of Ni, Ti, O, Cl, C and N with a Ni/Ti atomic ratio of ~2.31, approximately matching with the nominal ratio (Ni/Ti = 2 : 1) and the related data are listed in Table 1. The EDX analysis yields slightly higher values for the Ni/Ti atomic ratio of LDH powder than the nominal Ni/Ti ratio used, which may be due to the formation of mixed oxides of Ni(Ti)O, combined with Ti free NiO phases, also evident from the XPS observations. Although the synthesis of Ni/Ti LDH is carried out at a comparatively low temperature (130 °C), the formation of Ni(Ti)O cannot be ruled out. The synthesis was carried out using water soluble Ni(NO<sub>3</sub>)<sub>2</sub>·6H<sub>2</sub>O (with NiO<sub>x</sub> as a minor impurity) and hygroscopic TiCl<sub>4</sub>, which at room temperature (~25 °C) produces titanium oxychloride, titanium dioxide and dense white fumes of hydrochloric acid in an aqueous medium. The presence of NiO<sub>x</sub> as an impurity is evident from XRD and XPS observations of Ni/Ti LDH. The XPS analysis also reveals the surface reduction of Ti<sup>4+</sup> species to Ti<sup>3+</sup> accompanied by oxygen vacancies. The EDX also indicates the atomic ratio of Ni/Ti to be fractionally higher (2.31 : 1) than the expected stoichiometric ratio of 2 : 1 for Ni/Ti. Thus, based on the nature of chemicals used, XRD, XPS and EDX observations, it is concluded that some amount of mixed oxide Ni(Ti)O is formed during the hydrothermal synthesis of Ni/Ti LDH.

The presence of Cl in the EDX analysis (also observed in the XPS) might have resulted from the use of TiCl<sub>4</sub> as the precursor of Ti in the synthesis of Ni/Ti LDH. However, no role of Cl in the Ni/Ti LDH formation is envisaged.

### 3.6. N<sub>2</sub> adsorption/desorption measurements

In order to gain insight into the specific surface area and porosity of the LDH, low temperature N<sub>2</sub>-adsorption–desorption measurement was carried out (Fig. 9). The BET isotherm belonged to type IV with H3-type hysteresis loop ( $p/p_0 > 0.4$  to ~0.8). The considerably large hysteresis loop shows that the condensation of N<sub>2</sub> inside the pores and their release following a reduction in pressure follow different paths, a characteristic of the mesoporous structure of the material.<sup>9,10</sup> The Ni/Ti LDH thus consists of uniform mesopores formed through accumulation of particles. A broad pore size distribution is observed for the LDH sample with an average pore width of 4.58 nm, which is likely to have been originated due to the use of urea as a template during the hydrothermal treatment. The BET specific surface area of 230 m<sup>2</sup> g<sup>-1</sup> for the LDH could be considered as quite high, due to which higher photocatalytic efficiency was observed. The synthesis of Ni/Ti LDH uses urea as the template, which hydrolyses during the hydrothermal reactions giving ammonium and carbonate ions. The presence of CO<sub>3</sub><sup>2-</sup> in the interlayer positions, confirmed by other experimental results, makes the substance porous and is responsible for the comparatively large surface area of Ni/Ti LDH.

The BJH adsorption and desorption cumulative pore volume was 0.235 and 0.215 cm<sup>3</sup> g<sup>-1</sup> respectively. The pore size distribution in the synthesized LDH is dominated by both micropores and mesopores in the diameter range of 0–10 nm. Therefore, the specific architecture of 2 : 1 Ni/Ti LDH consists of hexagonally oriented assemblies of LDH nanocrystals on the urea substrate. The mesoporous nature of the material with an

appropriate spatial arrangement is likely to assist electron/hole transfer within the framework and is therefore likely to be photocatalytically active.<sup>2,9,19,20</sup>

### 3.7. XPS analysis

The surface characterization of 2 : 1 Ni/Ti LDH was performed by XPS. Fig. 10–16 show the XPS patterns of Ni/Ti LDH. The chemical states of the elements were identified by comparison of the obtained photoelectron binding energies (BE) with those taken from the literature. The XPS full surface survey spectrum testifies the presence of different elements on the surface of the LDH and also reveals the presence of surface states of metals with oxygen vacancies. Fig. 10 shows photoelectron lines at binding energies of about 199, 289, 402, 455.2, 531 and ~854.2–885 eV which can be attributed to Cl 2p, C 1s, N 1s, Ti 2p, O 1s and Ni 2p respectively.

The Ni 2p<sub>3/2</sub> regions for the synthesized LDH show the presence of peaks (Fig. 11) in the range of 854.2–870 eV. The first peak around 854.2 eV is attributed to Ni<sup>2+</sup> ions within the NiO phase. The second peak around 857.4 eV is attributed to Ni<sup>2+</sup> ions within the composite oxide structure. Meanwhile, the other two peaks, which lie at *ca.* 863.4 eV and 867.6 eV above the first and second peaks respectively are assigned to their corresponding shake-up satellite lines.<sup>20</sup> The region from 871.6 eV to 885 eV represents the Ni 2p<sub>1/2</sub> region. The peak at 873.2 eV fits very well the previously reported results for zero-valent metallic nickel Ni(0), whereas the peak at 882 eV is assigned to its corresponding shake-up satellite lines. The detection of metallic nickel Ni(0) clearly indicates a reduction of the Ni<sup>2+</sup> species on the surface of the LDH.<sup>21</sup>

In the high resolution O 1s spectrum region, two peaks O<sub>I</sub> and O<sub>II</sub> are observed representing two different kinds of surface oxygen species (Fig. 12). This is found to be in agreement with the literature and the present result that the O<sub>I</sub> with the lower BE of around 529.6 eV is characteristic of the lattice oxygen bound to metal cations of the structure, while O<sub>II</sub> with the higher BE of around 530.8 eV most likely belongs to surface oxygen, including mainly the oxygen species of hydroxyl groups.<sup>22</sup>

The high resolution XPS spectrum of Ti 2p (Fig. 13) shows evidence of two asymmetric peaks at binding energies of 455.2 eV and 461.5 eV corresponding to Ti 2p<sub>3/2</sub> and Ti 2p<sub>1/2</sub> states of Ti. Thus the surface shows the presence of two titanium species. Apart from the contributions from Ti<sup>4+</sup> species, shoulders associated with Ti 2p<sub>3/2</sub> and Ti 2p<sub>1/2</sub> peaks at binding energies of 457.9 eV and 463.8 eV can be attributed to Ti<sup>3+</sup>, as observed in previous studies.<sup>21–24</sup> This surface reduction indicates the presence of negatively charged oxygen vacancies in the surface region, the negative charge being shared by titanium cations adjacent to the defect sites.

The high resolution N 1s region (Fig. 14) shows the existence of two peaks at binding energies 403 eV and 405 eV respectively. The binding energy of the N 1s line is very sensitive to the chemical environment of the nitrogen atom and it varies from 396 eV to 408 eV.<sup>25</sup> The 403 eV peak is associated with terminally bonded well screened molecular nitrogen ( $\gamma$ -N<sub>2</sub>), and the 405 eV peak is due to terminally bonded poorly screened molecular nitrogen ( $\gamma$ -N<sub>2</sub>). Thus the spectroscopic features of the N 1s XPS spectra showed striking



similarity with the chemisorbed states of nitrogen as discussed in the previous literature.<sup>26</sup> Meanwhile, the small peak at 407.2 eV corresponds to  $\text{NO}_3^-$  present as an impurity on the surface due to the use of nickel nitrate for synthesizing the Ni/ Ti LDH.<sup>26,27</sup>

On comparison of the binding energy positions of the carbon components of previous studies with the high resolution C 1s spectrum of the synthesized LDH (Fig. 15), it is assigned that the peak at a binding energy of 289.2 eV is due to the presence of  $\text{CO}_3^{2-}$  species in the interlayer gallery of LDH. The identification of C and N peaks in the XPS spectra is due to the use of urea as a template in the hydrothermal synthesis.

Fig. 16 shows the XPS spectrum of Cl 2p clearly indicating two peaks at 198.2 eV and 199.3 eV from the Cl 2p core-level electrons. The strong peak at 198.2 eV represents the  $2p_{3/2}$  spin state, which could be assigned to  $\text{Cl}^-$  ions physisorbed on the Ni/Ti LDH surface, while the minor peak located at 199.3 eV represents the  $2p_{1/2}$  state that might be assigned to the Cl incorporated into the lattice of the LDH. The presence of these two peaks indicates that chlorine was incorporated into the lattice of the synthesized LDH as a result of the use of  $\text{TiCl}_4$  during hydrothermal treatment.

### 3.8. Optical properties

The diffuse reflectance UV–vis analysis (Fig. 17) was carried out to investigate the nature and coordination state of nickel and titanium incorporated into the layered framework. The hump at ~250 nm can be attributed to transitions. The strong absorption band in the region of 325 nm can be assigned to typical Ni(II) co-ordinated to the  $\text{CO}_3^{2-}$  gallery.<sup>1,9</sup> Meanwhile, a broad absorption band from ~400 to 700 nm is observed with maxima at ~550 nm indicating the presence of  $\text{Ti}^{4+}$  in the brucite like sheets. The broad nature of absorption at ~550 nm could be ascribed to supramolecular guest–guest (hydrogen bonding and van der Waals forces) or guest–host interactions (electrostatic attraction, hydrogen bonding and van der Waals forces). In the case of layered materials, the UV spectrum shows an overall broadening and a red shift is observed due to higher aggregate formation.<sup>28–30</sup>

**3.8.1. Comparative UV-Vis DRS analysis**—The solid UV-vis DRS spectra measured at room temperature for the synthesized 2 : 1 Ni/Ti LDH and commercial catalysts like ZnO, ZnS,  $\text{TiO}_2$  and Degussa P25 are shown in Fig. 18. All of them showed strong absorbance at ~270–460 nm. However, the synthesized LDH exhibits a stronger absorption band from ~400 to 700 nm, which is not observed in any the commercial catalysts. The stronger absorbance in the visible region of the electromagnetic spectrum makes 2 : 1 Ni/Ti LDH a potential candidate for degradation of dyestuffs under visible light than that of the commercial catalysts like ZnO, ZnS,  $\text{TiO}_2$  and Degussa P25.

**3.8.2. Band gap calculation**—UV–vis absorption measurement is a convenient and effective method for explaining the band structure of semiconductor materials. For a better understanding of the semiconducting properties of Ni/Ti LDH, the band gap of 2 : 1 Ni/Ti LDH and that of some commercial catalysts were measured from a solid UV–Vis diffuse reflectance study (Fig. 19) using the following classical Tauc approach.<sup>17</sup>

$$\alpha E_p = K(E_p - E_g)^n \quad (1)$$

where  $E_g$  represents the optical band gap,  $E_p$  is the photon energy,  $K$  is a constant and  $n$  depends on the nature of the transition. In fact,  $n$  assumes a value of 1/2, 3/2, 2, and 3 for direct allowed, direct forbidden, indirect allowed and indirect forbidden transitions respectively. In the case of 2 : 1 Ni/Ti LDH, the best fit of  $(\alpha E_p)^2$  versus  $E_p$  was obtained for  $n = 1/2$ , suggesting allowed direct transitions across the energy band gap. The extrapolated value (the straight line to the  $X$ -axis) of  $E_p$  at  $\alpha = 0$  gives absorption edge energies corresponding to  $E_g = 2.68$  eV for 2 : 1 Ni/Ti LDH. This value is much smaller than that of pure NiO (~2.93), ZnO (~3.21 eV), ZnS (~3.54 eV), TiO<sub>2</sub> (~3.22 eV) and Degussa P25 (~3.19 eV). The smaller band gap imparts better semiconducting properties to Ni/Ti LDH in comparison with photocatalysts like ZnO, ZnS, TiO<sub>2</sub>, NiO and Degussa P25.<sup>8</sup> Moreover, the red shift in the UV-visible absorption spectrum of the Ni/Ti LDH is attributed to the narrow band gap. This suggests that pairs can be generated, even though the particle is irradiated with long wavelength visible light.<sup>8,31</sup> The decrease of band gap can be due to the localized gap states induced by Ti<sup>3+</sup>. The decrease in band gap has also been attributed to oxygen vacancies, which are responsible for its unique properties in photocatalytic applications. Thus, the Ni/Ti LDH material is expected to show more activity in the visible region of the electromagnetic spectrum and hence was used for dye degradation under visible light.

### 3.9. Zeta potential measurements

The change in the surface charge of the aqueous LDH was monitored using zeta potential measurements in aqueous media (Fig. 20) which revealed variation of surface charge of Ni/Ti-LDH at different pH. It is observed that the zeta potential of Ni/Ti LDH decreased monotonically with increasing pH, attaining zero charge at pH 6.92, which could therefore be identified as the isoelectric point of the synthesized LDH.<sup>31,32</sup> Thus, the cationic dye MB would be electrostatically attracted on the catalyst surface at pH > pH<sub>(zpc)</sub> values where its zeta potential values are negative, furnishing higher degradation efficiency.

### 3.10. Photoluminescence analysis

Photoluminescence (PL) is primarily used to understand the fate of electron-hole pairs in semiconductors as well as to examine the effectiveness of trapping, migration and transfer of charge carriers. In this study (Fig. 21), the PL technique is used in order to obtain a better understanding of the optical properties, surface states, oxygen vacancies and defects present in the synthesized LDH. Present-day research studies have validated that Ti incorporated photocatalytic systems show significant excitonic PL emissions resulting from the surface defects that strongly influence photocatalytic activities. The synthesized LDH material showed good PL emission intensities which are attributed to the presence of either oxygen vacancies and/or defects in the LDH material that lead to a significant increase in its optical properties. Oxygen vacancies and defects were reported to bind the photo-induced electrons easily to form excitons, so that the PL signal can occur easily. Therefore, the PL signal is found to increase with the increasing content of oxygen vacancies or defects.<sup>33,34</sup> It is seen that upon excitation of the LDH at 350 nm, several excitonic PL emission bands are

observed at ~389 nm, 442 nm, and a broad band at ~495 nm, which is accompanied by a valley extending up to 630 nm, respectively, results from the surface oxygen vacancies and defects of the sample. This observation is in accordance with the UV-vis DRS observations and a number of earlier reports.<sup>27–30</sup> Thus, the surface states and inner structures of Ni/Ti LDH are likely to play a vital role in its photocatalytic activities.

### 3.11. Photocatalytic reactions

The photocatalytic activity of a semiconductor material is dependent on the surface area, the narrow band gap, the light harvesting ability and the separation of  $e^-h^+$  pairs by absorbing the incident photons with energies larger than its band gap energy ( $E_g$ ). The PL spectra support a stronger ability for pair separation in 2 : 1 Ni/Ti LDH. The high specific surface area, the narrow band gap and the presence of variable surface states accompanied by oxygen vacancies, as is evident from BET, DRS and XPS analyses, indicate that the synthesized LDH material could be induced easily with visible light, to produce more photo-induced carriers, resulting in high visible light photocatalytic activity. In the photocatalytic reactions, 2 : 1 Ni/ Ti LDH photocatalyst was dispersed in 200 ml aqueous solution of methylene blue and the mixture was stirred vigorously for 30 min in the dark for establishing adsorption equilibrium and then was exposed to irradiation by visible-light. The synthesized LDH exhibited better photocatalytic degradation of MB than commercial catalysts like ZnO, ZnS, TiO<sub>2</sub>, NiO and Degussa P25. The degradation experiments were performed separately by varying the catalyst dose, the dye concentration and the pH. The photocatalytic degradation was estimated from the decrease in the absorption intensity of MB at  $\lambda_{max} = 664$  nm at 15 min intervals and the absorption spectra of the mixture were monitored as functions of irradiation time using a UV-Vis spectrometer (Shimadzu 1800). The extent of decomposition of the dye was obtained from the ratio  $C/C_0$ , where  $C$  and  $C_0$  are the absorbances at a particular time interval and at  $t = 0$  respectively. It is seen that the strong absorption bands of MB decreased gradually upon increasing the irradiation time, and the absorbance of the dye solution was close to zero after 75 min of visible light irradiation for the synthesized LDH (Fig. 22). In addition, the solution colour changed from an initial blue to nearly transparent at the end of the degradation. The enhanced photocatalytic activity of the synthesized Ni/Ti LDH, compared to ZnO, ZnS, TiO<sub>2</sub>, NiO and Degussa P25, can be explained by the presence of high surface area, defects, oxygen vacancies and Ti<sup>3+</sup> centers associated within the layered brucite like structure as supported by BET, DRS, PL and XPS analyses.<sup>15,23,34,35</sup> Blank reactions (without a catalyst) as well as dark reactions (in the dark) were also performed under the same experimental conditions. Negligible degradation of MB was observed in the absence of the photocatalyst or visible light irradiation, which indicates that visible light plays a vital role in the photodegradation process.

**3.11.1. Effect of photocatalyst dose**—The influence of the catalyst amount on decolorization of MB under visible light using 2 : 1 Ni/Ti LDH catalyst was studied by varying the amount of catalyst between 5.0 mg and 20 mg at  $1 \times 10^{-6}$  M (= 0.3198 mg L<sup>-1</sup>) MB concentration (Fig. 23). The results showed that on increasing the amount of catalyst from 5 to 20 mg in 200 ml of aqueous MB, an increase in decolorization efficiency was observed from 66% to 99.8% respectively. The increase in decolorization efficiency with increasing the amount of catalyst dose in the reaction resulted from an increase in the

available surface area or the active sites of the catalyst. However, the decrease in the degradation efficiency on increasing the catalyst load further to  $0.1 \text{ g L}^{-1}$  could be attributed to deactivation of activated molecules by collision with ground state molecules of the catalyst. Following this observation, the catalyst amount was kept at the value of 15 mg in subsequent photocatalytic degradation experiments for obtaining the maximum degradation efficiency.

**3.11.2. Effect of pH**—The pH of a dye solution is an important parameter which controls the rate of degradation. In order to study the effect of pH, degradation experiments were carried out using 15 mg of  $1 \times 10^{-6} \text{ M}$  ( $= 0.3198 \text{ mg L}^{-1}$ ) MB solution (Fig. 24) within the pH range of 5.0 to 11.0 by the addition of either HCl or NaOH (0.1 M). The relationship  $C/C_0$  of aqueous MB was observed by varying the pH and is presented in Fig. 24. When the pH of the solution was increased from 5.0 to 6.0, the removal of MB increased from 36% to 41%. The maximum MB degradation of  $\sim 99.8\%$  was observed at pH 11.0, which is found to be in good agreement with previous studies.<sup>31,33</sup> The pH determines the surface charge on the catalyst surface. The degradation efficiency was found to be low in acidic media. This is because at low pH, the  $\text{H}^+$  ion was considered to be a competitor to MB for adsorption sites on the surface of the catalyst. Moreover, as is evident from the zeta potential results, the surface of the LDH was also positively charged at low pH values which created electrostatic repulsion with the dye molecules. As a result, the degradation of MB could not be enhanced to a greater extent. However, in alkaline medium, at pH higher than that of zpc, the catalyst surfaces attain negative zeta potential values and were electrostatically attracted to the MB molecules having electropositive charge, which led to the increase in the degradation efficiency.

**3.11.3. Effect of the initial dye concentration**—It is important from mechanistic as well as application points of view to study the dependence of the dye concentration on the photocatalytic degradation rate. The effect of the initial MB dye concentration on the degradation rate was investigated in the concentration range of  $1 \times 10^{-4}$ ,  $1 \times 10^{-5}$  and  $1 \times 10^{-6} \text{ M}$ , maintaining the other reaction parameters constant (pH = 11; catalyst = 15 mg in 200 ml MB) (Fig. 25). It is found that with  $1 \times 10^{-6} \text{ M}$  MB concentration,  $\sim 99.8\%$  degradation was achieved. Beyond this concentration, the degradation rate decreased to 78% and 92% respectively for  $1 \times 10^{-4} \text{ M}$  and  $1 \times 10^{-5} \text{ M}$  MB. This may be due to the following factors: (i) higher dye concentration might serve as the inner filter shunting the photons away from the catalyst surface; (ii) non-availability of oxidative free radicals; (iii) more number of dye molecules get adsorbed on the catalyst surface, thus blocking the surface active sites from participating in the degradation process. Thus, the MB concentration was kept at  $1 \times 10^{-6} \text{ M}$  ( $= 0.3198 \text{ mg L}^{-1}$ ) in photocatalytic degradation experiments for obtaining the maximum efficiency.

**3.11.4. Catalyst recyclability and photostability**—After each reaction run, the catalyst was separated from the reaction system and its reusability was also investigated carefully. The catalyst was washed three times with water, dried and reused. The degree of MB degradation for the first cycle was  $\sim 99.8\%$  (Fig. 26). Although the degradation ability of the catalyst declined to  $\sim 92\%$ , 88%, 86% and 80% respectively for the second, third, fourth

and fifth cycles when they were reused again, the degradation rate still could amount to 80% after repeating the fifth catalytic procedure, suggesting that the synthesized LDH is a potential recyclable candidate for dye degradation purposes.

In order to understand the photostability of the Ni/Ti LDH, the FT-IR analysis of the synthesized 2 : 1 Ni/Ti LDH and that recovered at the end of the fifth cycle of MB degradation was performed (Fig. 27). The presence of all the characteristic IR-bands in the same position, with some minor changes in the fingerprint region, after the fifth catalytic cycle indicated that the catalyst is of excellent stability under visible light irradiation.<sup>8,32–34</sup>

**3.11.5. Role of reactive species**—The active species participating in the photodegradation process were studied indirectly by the addition of scavengers into the reaction mixture separately at the beginning of the dye degradation experiments in order to elucidate the mechanism of photocatalysis.<sup>30–33</sup> The roles played by the main active species in the photodegradation of dyes, being  $\cdot\text{OH}$ ,  $h^+$  and  $\text{O}_2^{\cdot-}$  species, were investigated indirectly through radical and hole trapping experiments and are illustrated in Fig. 28. It was observed that MB degradation (~38%) was suppressed upon the addition of *n*-butanol (a scavenger of  $\cdot\text{OH}$ ), indicating that dissolved  $\cdot\text{OH}$  radicals were the dominant active species in this process. In contrast, the addition of disodium ethylenediaminetetraacetate ( $h^+$  scavenger) had a significant negative effect on the degradation of MB, as is evident from the  $C/C_0$  plot, where MB degraded ~52%, confirming that the holes were also the active species. However, MB degraded ~82% through the addition of benzoquinone (BQ) ( $\text{O}_2^{\cdot-}$  scavenger), indicating that  $\text{O}_2^{\cdot-}$  radicals were not the dominant active species in the MB photocatalytic degradation process by 2 : 1 Ni/Ti LDH. These results are in accordance with the XPS and PL observations, indicating that the photocatalytic process was mainly governed by direct  $h^+$  and  $\cdot\text{OH}$  radicals.

**3.11.6. Kinetics of photodegradation**—The kinetics of photodegradation of aqueous methylene blue was studied under optimum conditions (pH = 11; catalyst dose = 0.075 g L<sup>-1</sup>; MB concentration = 1 × 10<sup>-6</sup> M) to understand the reaction characteristics of MB on the Ni/Ti-LDH material. The linear relationship between  $\ln(C_0/C)$  and irradiation time (Fig. 29) suggests that the degradation of MB by the LDH photocatalyst follows pseudo first-order kinetics, which can be represented by the following equation:

$$\ln \left( \frac{C_0}{C} \right) = kt \quad (2)$$

where  $C_0$  is the initial concentration of the MB and  $C$  is the concentration at time  $t$ . The apparent rate constant  $k$  was calculated to be 0.0276 min<sup>-1</sup> and the half-life ( $t_{1/2}$ ) of the sample was found to be 25.11 min, which was calculated from  $k$  using the equation:

$$t_{1/2} = \frac{\ln 2}{k} \quad (3)$$

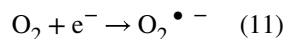
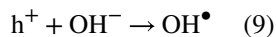
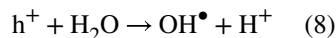
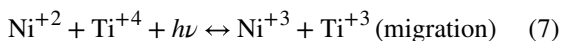
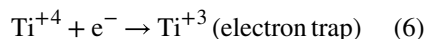
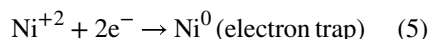
As a result, the photodegradation kinetics fitted well with the pseudo first-order model, indicating that the reaction rate is dependent on the light intensity and absorption performance of the catalyst.<sup>2,16</sup>

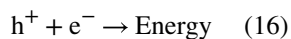
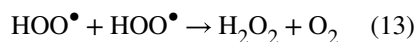
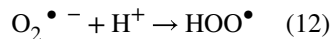
**3.11.7. Comparative study of the photocatalytic process**—A comparative study was undertaken to validate the influence of Ni/Ti LDH on the photocatalytic activity of MB [pH = 11; catalyst dose = 15 mg in 200 ml of aqueous MB; MB concentration =  $1 \times 10^{-6}$  M (= 0.3198 mg L<sup>-1</sup>)], which revealed an enhanced degradation of the aqueous methylene blue in comparison with some important commercial catalysts like ZnO, TiO<sub>2</sub>, ZnS and Degussa P25 (Fig. 30). The plot of  $C/C_0$  versus irradiation time revealed that Ni/Ti LDH displayed high photocatalytic activity under visible-light irradiation, reaching ~99.8% in 75 min, in comparison with that of other commercial catalysts (ZnO ~ 59%, ZnS ~ 49%, TiO<sub>2</sub> ~ 43%, NiO ~ 83% and Degussa P25 ~ 71% degradation respectively). Thus, Ni/Ti LDH showed higher photocatalytic activity in visible light than that of commercial catalysts.<sup>2,8,9</sup> Moreover, the blank reactions performed under the same set of experimental conditions without the catalyst showed ~15% adsorption, as is evident from the  $C/C_0$  plot against time, which is attributed to the effect of visible light exposure on adsorption of the dye. However, control experiments performed in the dark revealed ~23% adsorption as is evident from the  $C/C_0$  plot against time, indicating that visible light plays a major role in the degradation of aqueous methylene blue.

In order to elucidate whether adsorption or degradation occurred in the decolorization of aqueous methylene blue, comparative FT-IR analysis of the products of the dark reaction, the blank reaction and at the end of the decolourization processes of aqueous methylene blue with 2 : 1 Ni/Ti LDH were correlated with those of pure methylene blue (Fig. 31). All the characteristic IR bands of pure methylene blue were also observed in the same position in both blank and dark reactions. However, the peaks became broad particularly in the fingerprint regions, in the case of blank and dark reactions, indicating adsorption. The analysis of the FT-IR spectra of the aqueous MB solution at the end of the decolourization process after 75 min revealed the absence of most of the characteristic bands of methylene blue and some band shifts were observed in some cases, as is evident from Fig. 31, indicating that the methylene blue dye was totally degraded into simple molecules with 2 : 1 Ni/Ti LDH under visible light.

**3.11.8. Proposed mechanism of photodegradation**—On the basis of XPS, DRS and PL emission spectra, the pathway of the photodegradation of aqueous methylene blue by 2 : 1 Ni/Ti LDH has been suggested in light of the band theory by taking O-1s orbital as the valence band, and Ni-2p and Ti-2p orbitals as the conduction band. The entire degradation reaction is supposed to take place in a series of sequential reactions (eqn (4) to (16)) upon exposure to visible light at 30 °C. The electrons are excited from the valence band to the conduction band, leaving electron holes in the valence band. The excitation is initiated by the absorption of photons with energy equal to or greater than the band gap energy of the semiconductor material. It has been proposed that Ni/Ti LDH generates e<sup>-</sup>-h<sup>+</sup> pairs (eqn (4)) upon exposure to visible light. The photo-generated electrons reduce the Ni<sup>2+</sup> and Ti<sup>4+</sup> species present on the catalyst surface (electron trap) (eqn (5), (6)). Under vigorous stirring

in the presence of visible light, the lattice vibrations of the catalyst are intensified and the photogenerated electrons cause a strong redox reaction<sup>7,16,30–33</sup> (eqn (7)). The hopping holes move to the surface of the catalyst and react with water and OH<sup>-</sup> ions to yield OH<sup>•</sup> radicals (eqn (8), (9)). The photo-generated holes further degrade aqueous MB to simple molecules (eqn (10)). The electrons may react with adsorbed oxygen on the catalyst surface to produce superoxide (O<sub>2</sub><sup>•-</sup>) (eqn (11)). Superoxide (O<sub>2</sub><sup>•-</sup>) can further react with adsorbed H<sup>+</sup> to produce peroxide radicals (<sup>•</sup>OOH) (eqn (12)), further yielding H<sub>2</sub>O<sub>2</sub> (eqn (13)) and hydroxyl radicals (<sup>•</sup>OH) (eqn (14)). Hydroxyl (<sup>•</sup>OH) and superoxide (O<sub>2</sub><sup>•-</sup>) radicals are highly reactive species that will oxidize/degrade MB into simple molecules (eqn (15)). The photo-generated or hopping holes and electrons may further recombine and dissipate the energy as light or heat (eqn (16)) which will reduce the total quantum efficiency. The proposed photocatalytic pathway of degradation of aqueous MB with 2 : 1 Ni/Ti LDH involving the sequence of reactions is illustrated as follows:





The layered structure of the photocatalyst further assists in the electron–hole hopping conduction model. The XPS and the PL measurements suggest that Ni and Ti in the LDH are present in a number of oxidation states, accompanied by oxygen vacancies. The DRS band at ~400–700 nm (with a maximum at ~550 nm) indicates the presence of  $\text{Ti}^{4+}$  in brucite like sheets. The broad nature of absorption at ~550 nm could be ascribed to supramolecular guest–guest (hydrogen bonding and van der Waals forces) or guest–host interactions (electrostatic attraction, hydrogen bonding and van der Waals forces). The PL analysis indicates the presence of defects, because, on exciting the LDH at 350 nm, several excitonic PL emission bands are observed at ~389 nm and 442 nm and a broad band at ~495 nm accompanied by a valley extending up to 630 nm. These might have resulted from the surface oxygen vacancies and defects in the sample. On the basis of these data and the indirect trapping experiments, the mechanism of the photodegradation process has been presented in the form of an electron–hole hopping conduction model.

## 4. Conclusions

In summary, Ni/Ti-LDH on the urea substrate played a promising role as a semiconductor photocatalyst in which Ti atoms were dispersed homogeneously in the LDH lattice. The as-synthesized 2 : 1 Ni/Ti-LDH has been found to exhibit remarkable photocatalytic activity for the degradation of aqueous methylene blue under visible light in comparison with that of some important commercial photocatalysts like ZnO, ZnS,  $\text{TiO}_2$ , NiO and Degussa P25, due to its high specific surface area, porous structure, lower band gap, different surface states of Ni and Ti in the layered framework and the presence of defects, as confirmed by BET/BJH, DRS, XPS and PL observations. The photocatalytic activity improved in alkaline media particularly at pH 11, due to the electrostatic attractions between oppositely charged MB molecules and negatively charged Ni/Ti LDH catalyst in accordance with the zeta potential



results. The FT-IR analysis of the control experiments carried out in the dark and blank reactions (without a catalyst) with aqueous methylene blue showed adsorption, whereas degradation and decolorization of the dye marked the end of the reaction with the 2 : 1 Ni/Ti LDH photocatalyst under visible light. However, the catalyst retained its activity after five cycles of MB degradation, and the FT-IR analysis of the catalyst before and at the end of the fifth cycle showed excellent photostability. The pseudo first-order model satisfactorily described the photocatalytic reaction kinetics. The strategy of applying a urea solution as a basic precipitant and adding homogeneously dispersed Ti atoms can be extended to other transition metal-based oxide/hydroxide thin films to enhance their semiconducting properties. Therefore, it is expected that the Ni/Ti LDH in this work can be potentially used as an effective and recyclable visible-light photocatalyst for large scale environmental wastewater treatment.

## Supplementary Material

Refer to Web version on PubMed Central for supplementary material.

## Acknowledgments

The authors sincerely thank the Department of Physics and Meteorology, IIT Kharagpur, India for XPS measurements and the Central Instruments Facility, IIT Guwahati, India for SEM/ EDX and TEM analyses associated with this research work. The authors are also very grateful to the referees for suggesting certain important modifications to the manuscript.

## References

1. Parida KM, Mohapatra L. Chem Eng J. 2012; 179:131–139.
2. Silva CG, Bouizi Y, Fornes V, Garcia H. J Am Chem Soc. 2009; 131:13833–13839. [PubMed: 19725513]
3. Chen D, Li Y, Zhang J, Zhou JZ, Guo Y, Liu H. Chem Eng J. 2012; 185–186:120–126.
4. Xu S, Shen J, Chen S, Zhang M, Shen T. J Photochem Photobiol, A. 2002; 67:64–70.
5. Zhang LW, Fu HB, Zhu YF. Adv Funct Mater. 2008; 18:2180–2189.
6. Chen G, Qian S, Tu X, Wei X, Zou J, Leng L, Luo S. Appl Surf Sci. 2014; 293:345–351.
7. Xu ZP, Zhang J, Adebajo MO, Zhang H, Zhou C. Appl Clay Sci. 2011; 53:139–150.
8. Shao M, Han J, Wei M, Evans DG, Duan X. Chem Eng J. 2011; 168:519–524.
9. Choi H, Sofranko AC, Antoniou MG, Pelaez M, de la Cruz AA, Shoemaker JA, Dionysiou DD. Environ Sci Technol. 2007; 41:7530–7535. [PubMed: 18044537]
10. Senthilnathan J, Philip L. Chem Eng J. 2010; 161:83–92.
11. Comparelli R, Fanizza E, Curri ML, Cozzoli PD, Mascolo G, Agostiano A. Appl Catal, B. 2005; 60:1–11.
12. Zhang C, Gu L, Lin Y, Wang Y, Fu D, Gu Z. J Photochem Photobiol, A. 2009; 207:66–72.
13. Zhao YF, Wei M, Lu J, Wang ZL, Duan X. ACS Nano. 2009; 3:4009–4016. [PubMed: 19928881]
14. Zhang J, Fu D, Gao H, Deng L. Appl Surf Sci. 2011; 258:1294–1299.
15. Huang Z, Wu P, Gong B, Fange Y, Zhu N. J Mater Chem A. 2014; 2:5534.
16. Li K, Luo X, Lin X, Qi F, Wu P. J Mol Catal A: Chem. 2014; 383–384:1–9.
17. Ahmed AAA, Talib ZA, Hussein MZB. Appl Clay Sci. 2012; 56:68–76.
18. Li S, Bai Z, Zhao D. Appl Surf Sci. 2013; 284:7–12.
19. Zhu Y, Zhou Y, Zhang T, He M, Wang Y, Yang X, Yang Y. Appl Surf Sci. 2012; 263:132–138.
20. Galtayries A, Grimblot J. J Electron Spectrosc Relat Phenom. 1999; 98–99:267–275.
21. Wang H, Xiang X, Li F, Evans DG, Duan X. Appl Surf Sci. 2009; 255:6945–6952.

22. Fernández A, Rojas TC. *Mater Trans.* 2003; 44:2055–2061.
23. Price NJ, Reitz JB, Madix RJ, Solomon EI. *J Electron Spectrosc Relat Phenom.* 1999; 98–99:257–266.
24. Sambti M, Sangiovanni G, Granozzi G, Parmigiani F. *Phys Rev B: Condens Matter.* 1997; 55:7850–7858.
25. Tabet N, Faiz M, Al-Oteibi A. *J Electron Spectrosc Relat Phenom.* 2008; 163:15–18.
26. Baltrusaitis J, Jayaweera PM, Grassian VH. *Phys Chem Chem Phys.* 2009; 11:8295–8305. [PubMed: 19756286]
27. Mehta SK, Kumar S, Chaudhary S, Bhasin KK. *Nanoscale.* 2010; 2:145–152. [PubMed: 20648377]
28. Xu H, Zhang L. *J Phys Chem C.* 2010; 114:940–946.
29. Zou L, Xiang X, Wei M, Li F, Evans DG. *Inorg Chem.* 2008; 47:1361–1369. [PubMed: 18193827]
30. Khan MM, Ansari SA, Pradhan D, Ansari MO, Hang DH, Lee J, Cho MH. *J Mater Chem A.* 2014; 2:637–644.
31. Zhang C, Yang S, Chen H, He H, Sun C. *Appl Surf Sci.* 2014; 301:329–337.
32. Zou L, Xiang X, Fan J, Li F. *Chem Mater.* 2007; 19:6518–6527.
33. Cui GJ, Xu XY, Lin TJ, Evans DG, Li DQ. *Ind Eng Chem Res.* 2010; 49:448–453.
34. Yoshihara R, Katoh A, Furube Y, Tamaki M, Murai K, Hara S, Murata H, Arakawa M, Tachiya M. *J Phys Chem B.* 2004; 108:3817–3823.
35. Richardson IG. *Acta Crystallogr, Sect B: Struct Sci.* 2013; 69:414–417.

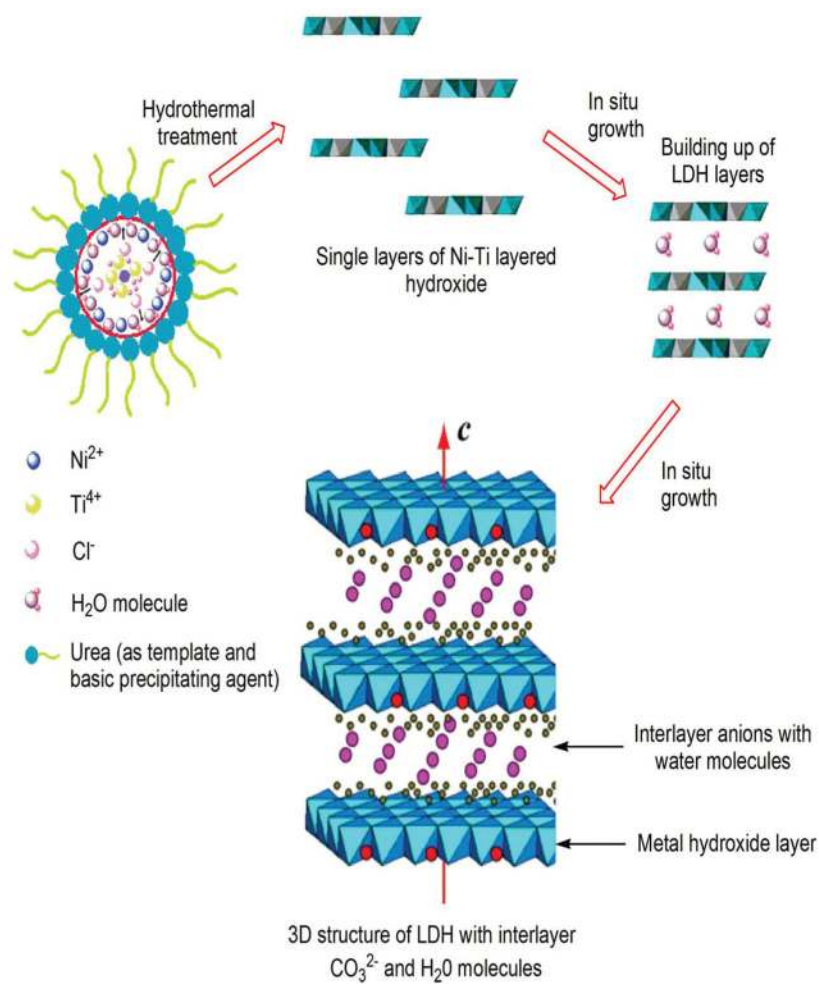


**Fig. 1.**  
Scheme of preparation of 2 : 1 Ni/Ti LDH.

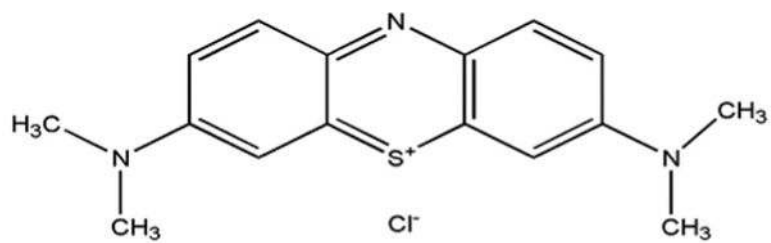


**Fig. 2.**  
Structure of methylene blue.

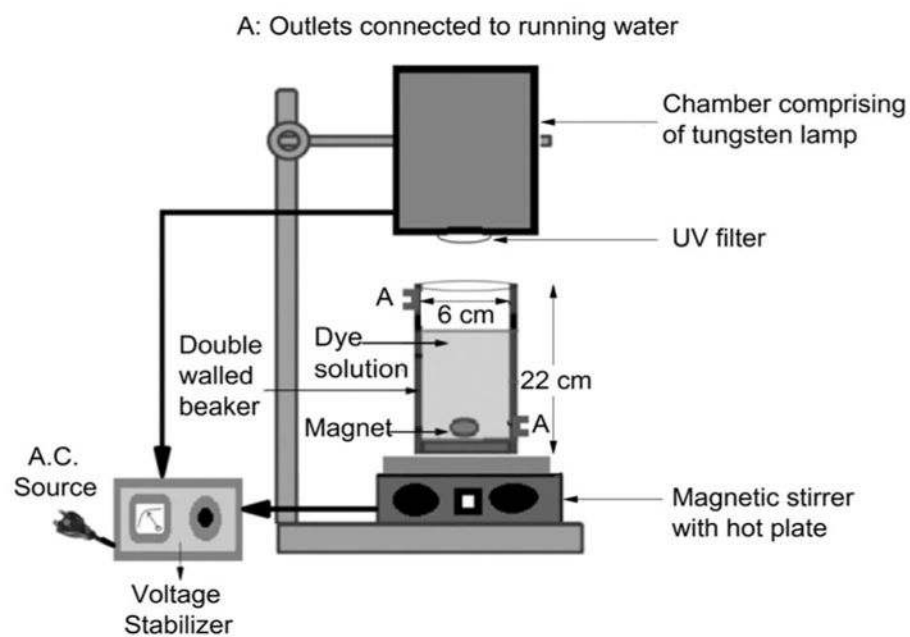


**Fig. 3.**  
Experimental setup for the visible light photodegradation of methylene blue.

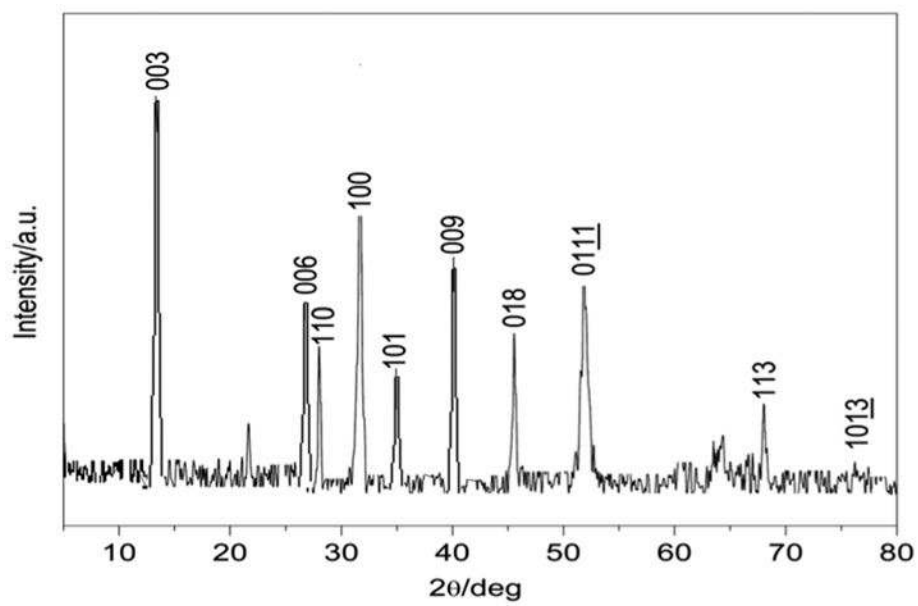


**Fig. 4.**  
XRD pattern of 2 : 1 Ni/Ti LDH.

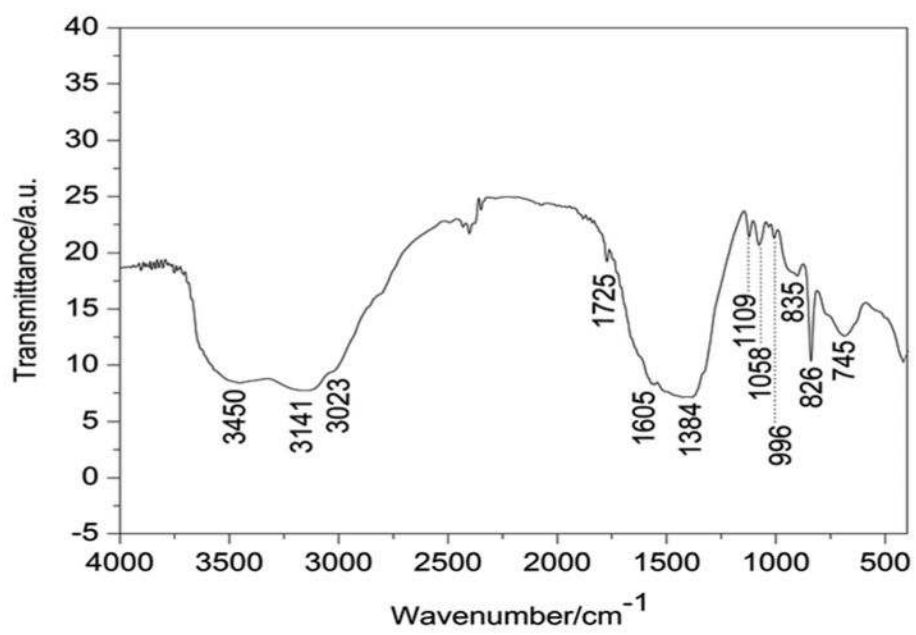


**Fig. 5.**  
FT-IR spectra of 2 : 1Ni/Ti LDH.

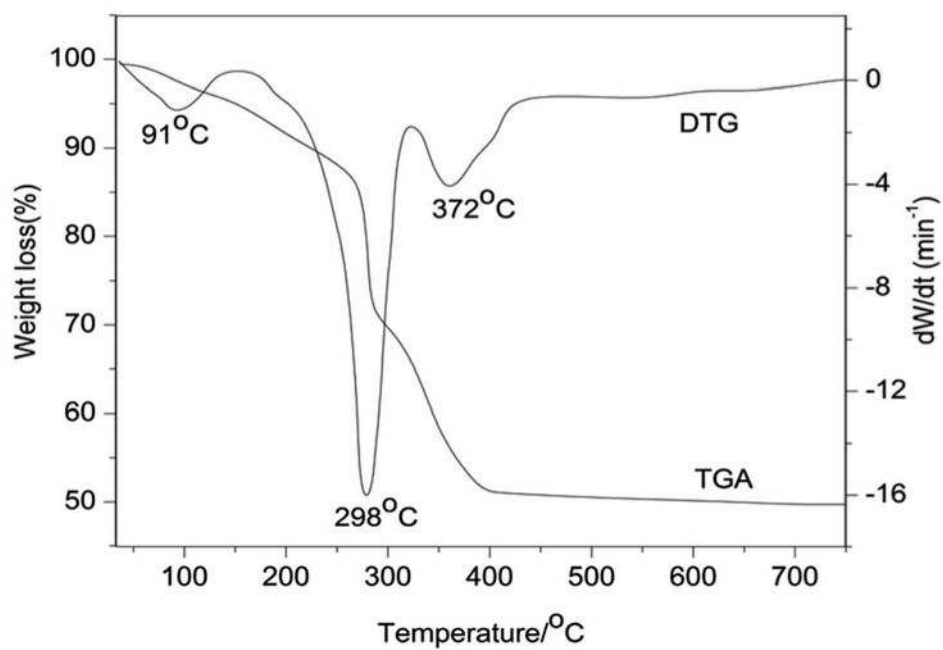


**Fig. 6.**  
TGA/DTG curve of 2 : 1 Ni/Ti LDH.



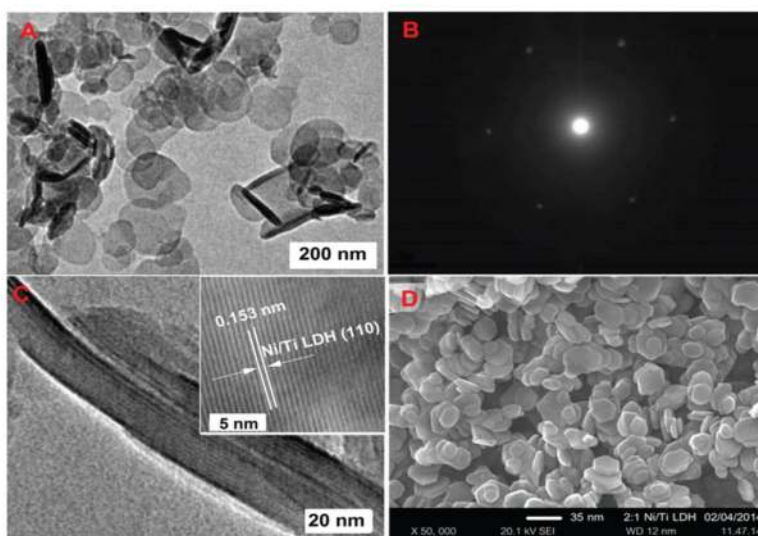


**Fig. 7.** (A) HR-TEM image of 2 : 1 Ni/Ti LDH. (B) SAED pattern of 2 : 1 Ni/Ti LDH. (C) High resolution micrograph showing the layered structure of 2 : 1 Ni/Ti LDH (the inset plot showing the interlayer distance between the periodic lattice fringes from the (110) plane of 2 : 1 Ni/Ti-LDH). (D) SEM image of 2 : 1 Ni/Ti LDH.

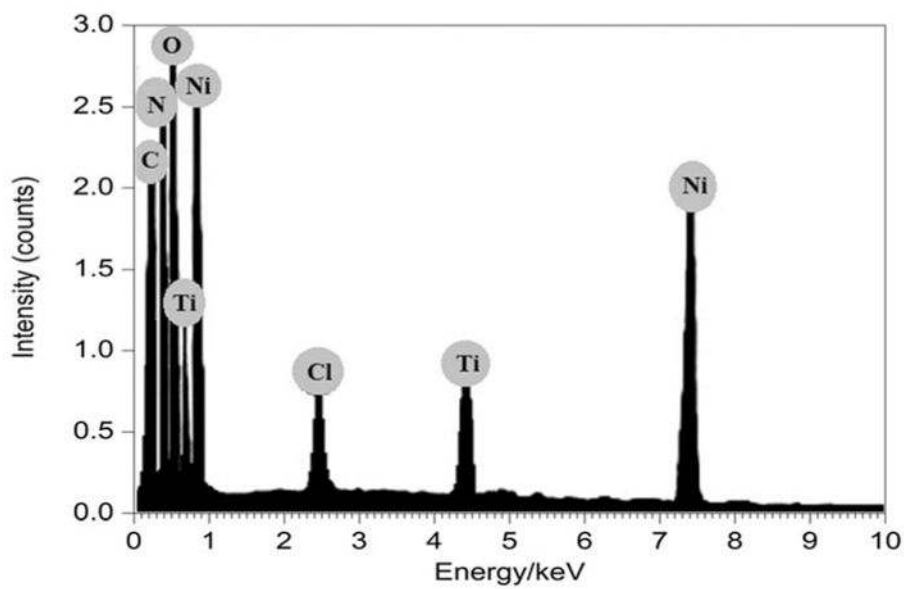


**Fig. 8.**  
EDX spectrum of 2 : 1 Ni/Ti LDH.

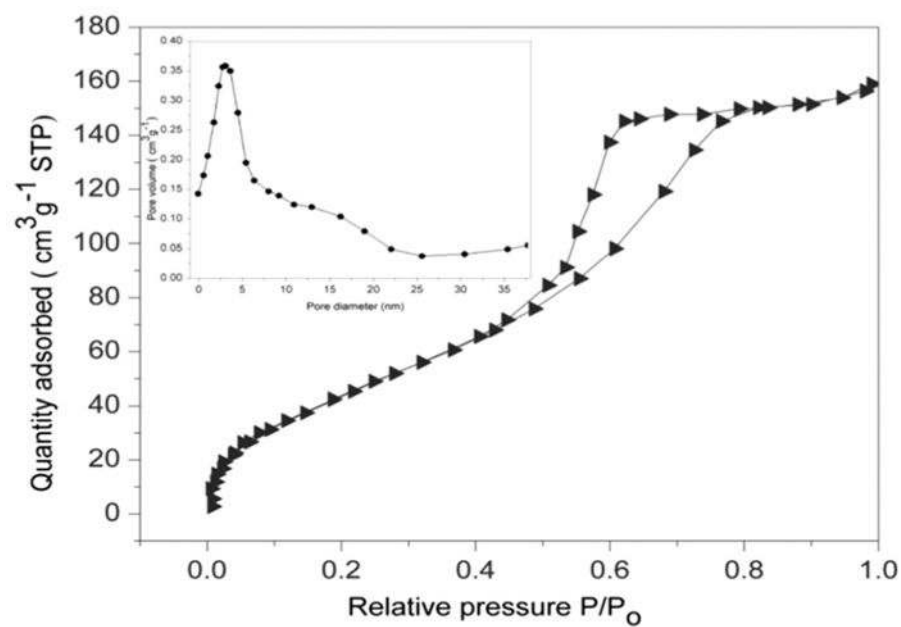


**Fig. 9.**  
 $\text{N}_2$  sorption isotherm of 2 : 1 Ni/Ti LDH.

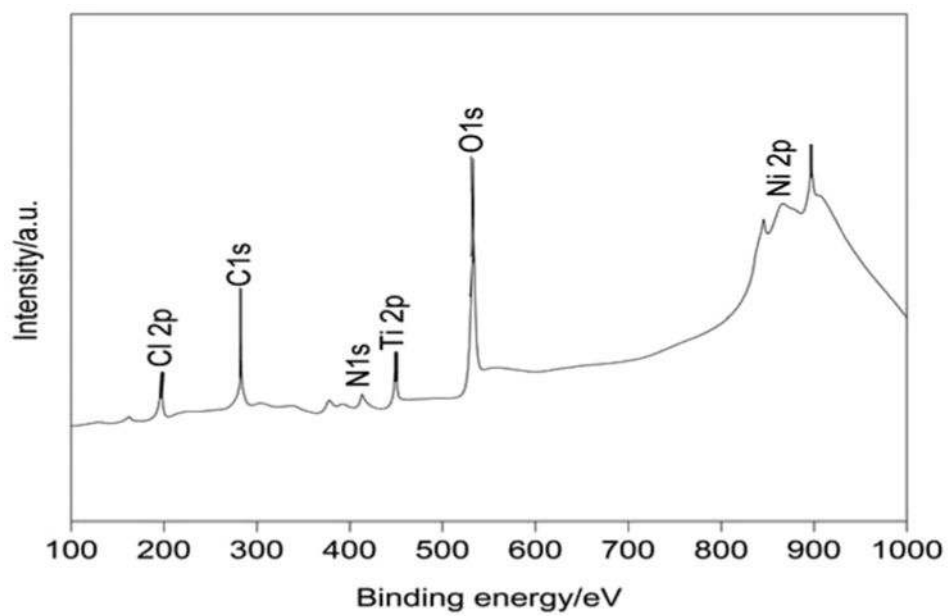


**Fig. 10.**  
XPS full survey of Ni/Ti LDH.

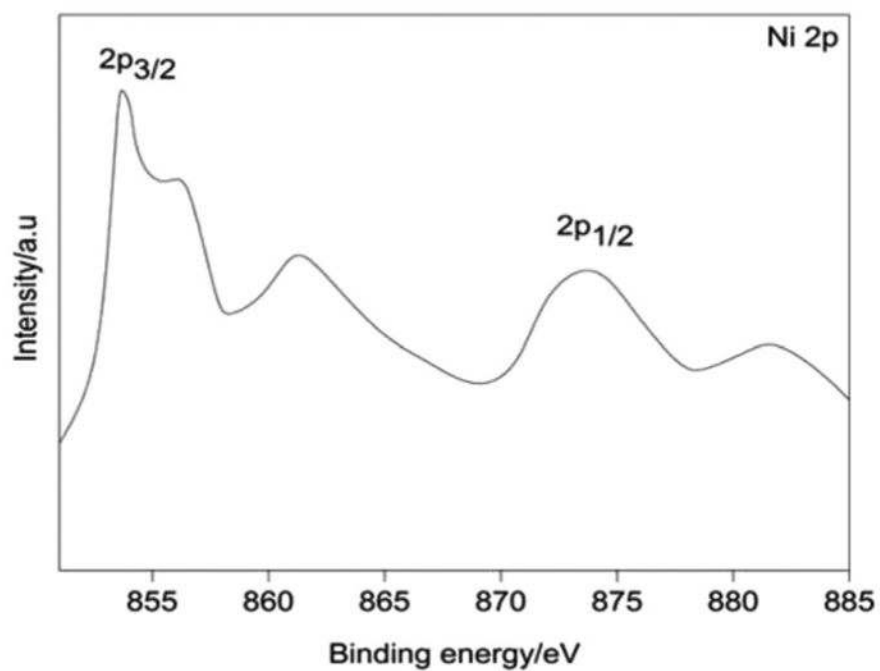


**Fig. 11.**  
XPS survey for Ni 2p.

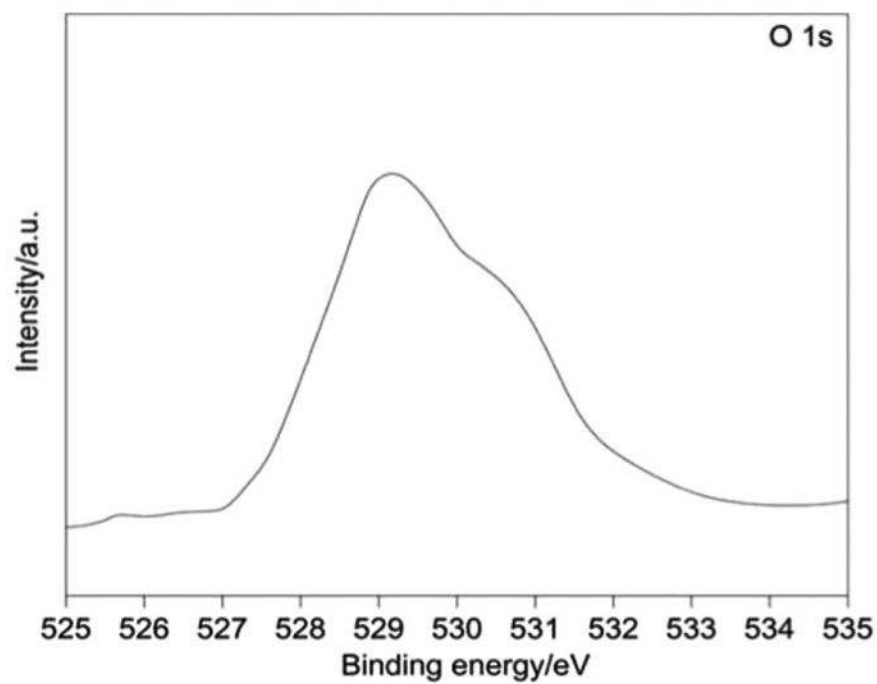


**Fig. 12.**  
XPS survey for O 1s.

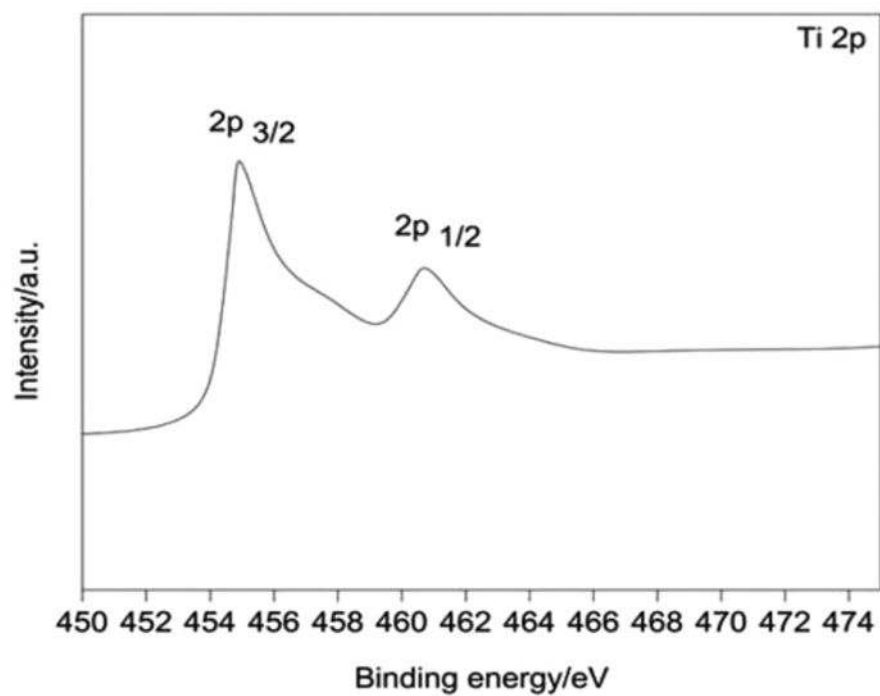


**Fig. 13.**  
XPS survey for Ti 2p.

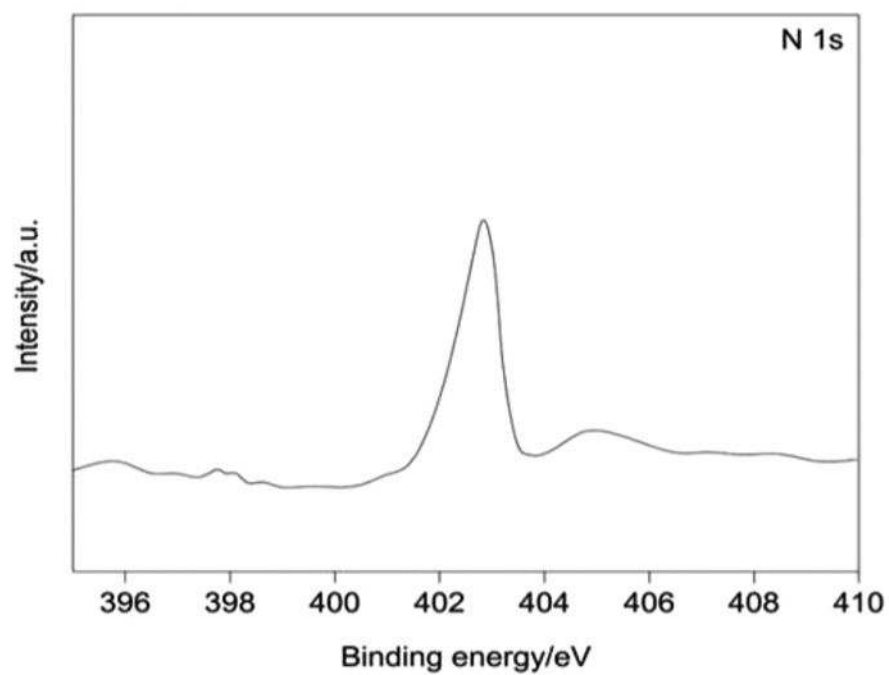


**Fig. 14.**  
XPS survey for N 1s.



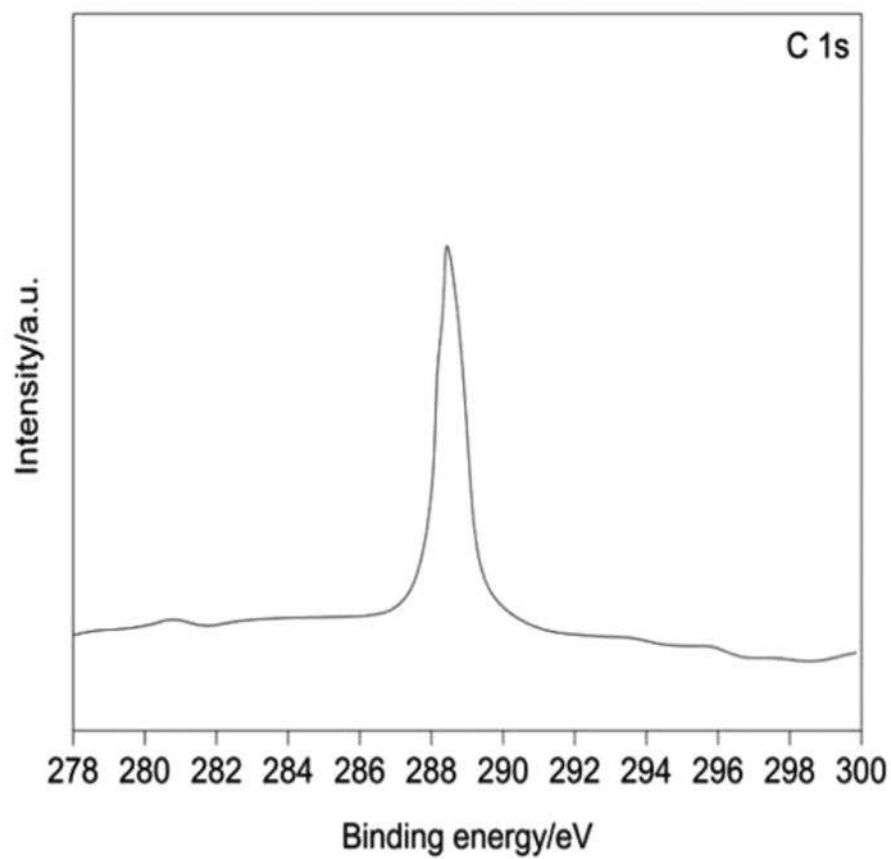


**Fig. 15.**  
XPS survey for C 1s.

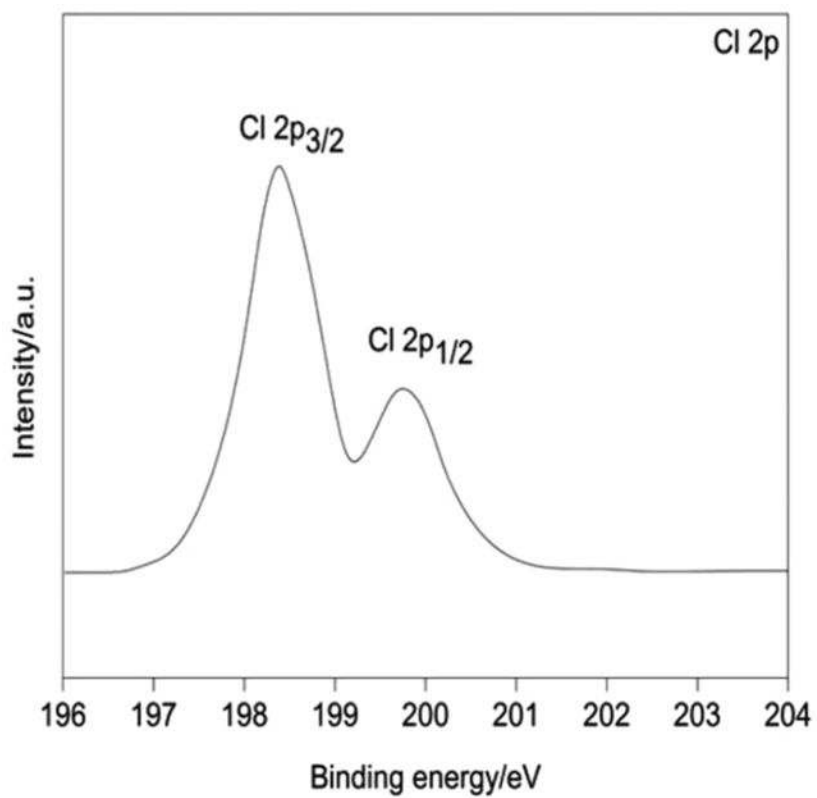


**Fig. 16.**  
XPS survey for Cl 2p.

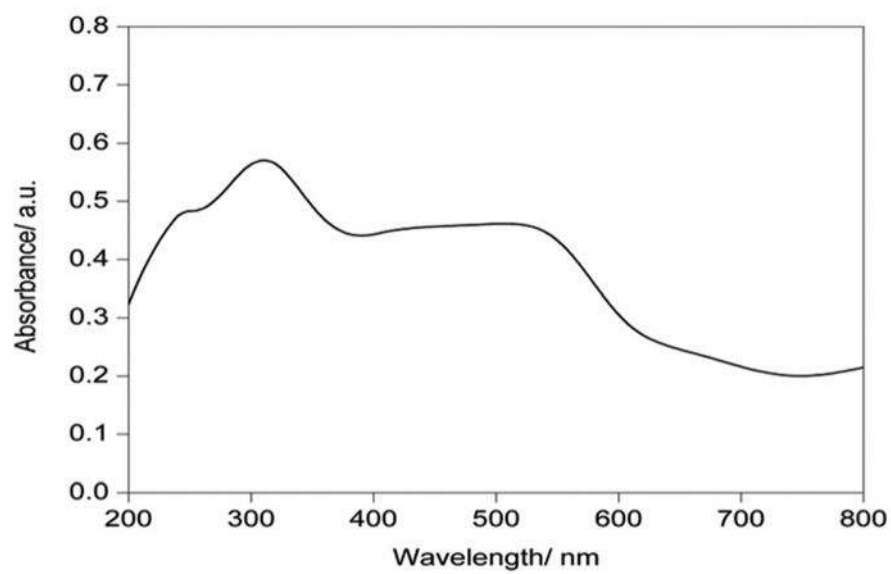


**Fig. 17.**  
Solid UV-Vis DRS spectra of 2 : 1Ni/Ti LDH.

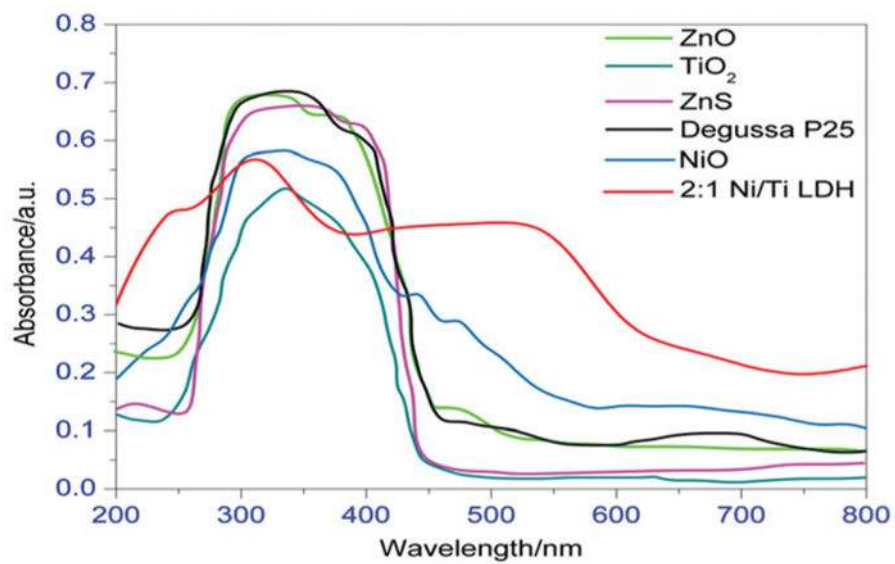


**Fig. 18.** Solid UV-Vis DRS spectra of 2 : 1 Ni/Ti LDH with some commercial catalysts.

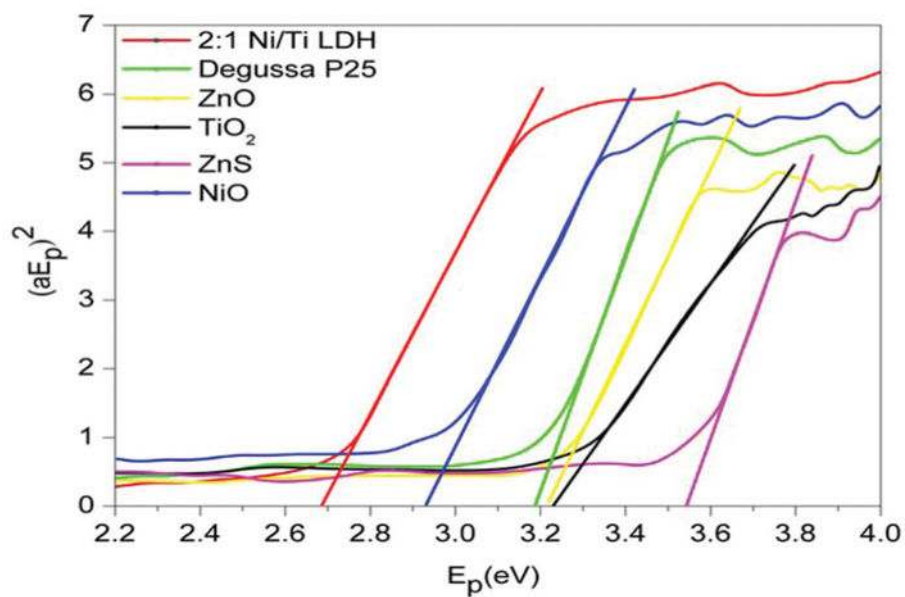


**Fig. 19.**  
Taucplots of 2 : 1 Ni/Ti LDH with some commercial catalysts.

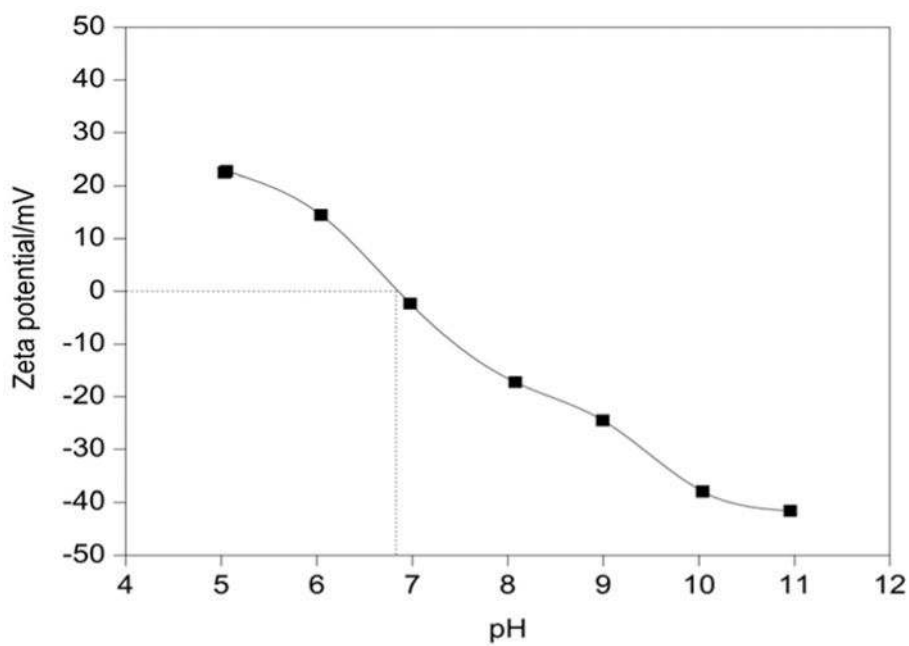


**Fig. 20.**  
Plot of the zeta potential of Ni/Ti LDH at different pH values.

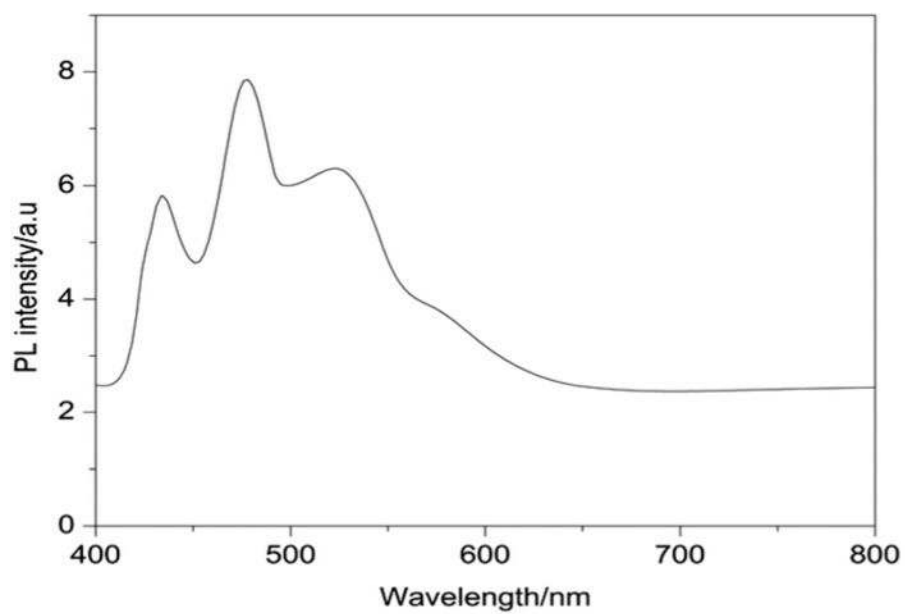


**Fig. 21.**  
Photoluminescence spectra of 2 : 1 Ni/Ti LDH.

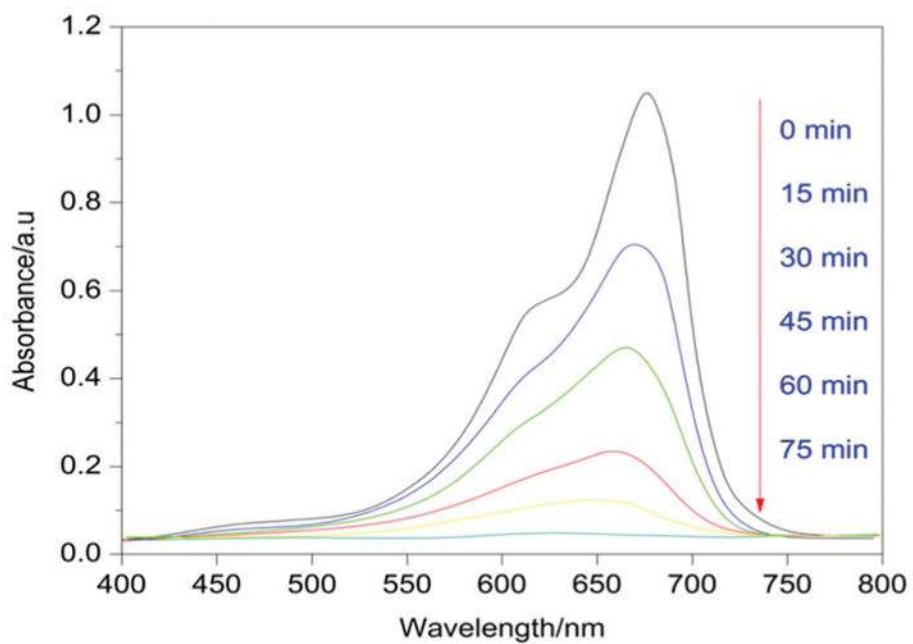


**Fig. 22.** UV absorption spectra involving the photodegradation of MB with 2 : 1 Ni/Ti LDH under visible-light [pH = 11; 15 mg of the catalyst;  $1 \times 10^{-6}$  M (= 0.3198 mg L<sup>-1</sup>) MB solution].



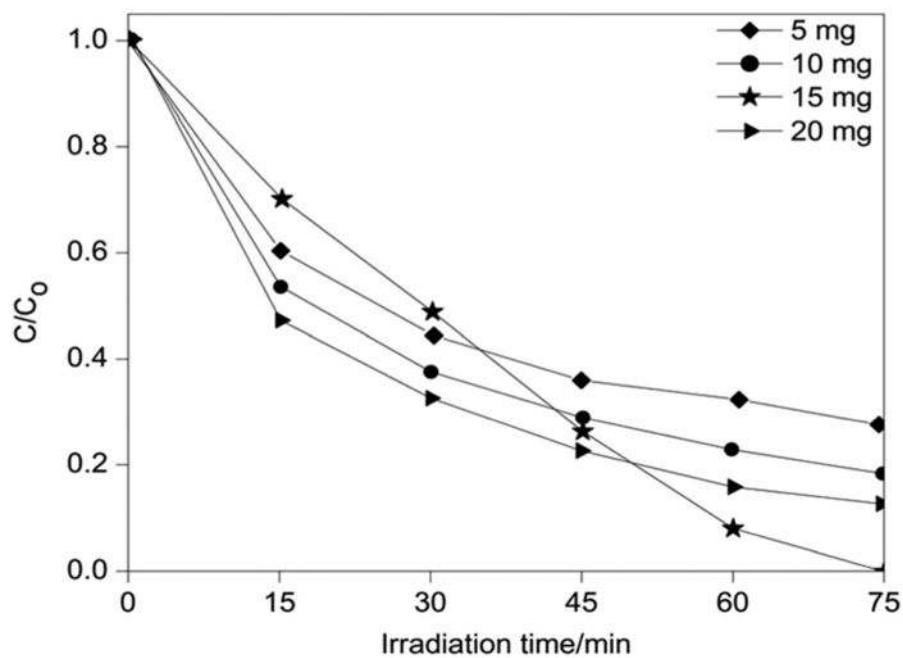


**Fig. 23.**

The effect of catalyst concentration on the photodegradation of MB [pH = 11; MB concentration =  $1 \times 10^{-6}$  M (= 0.3198 mg L<sup>-1</sup>)].

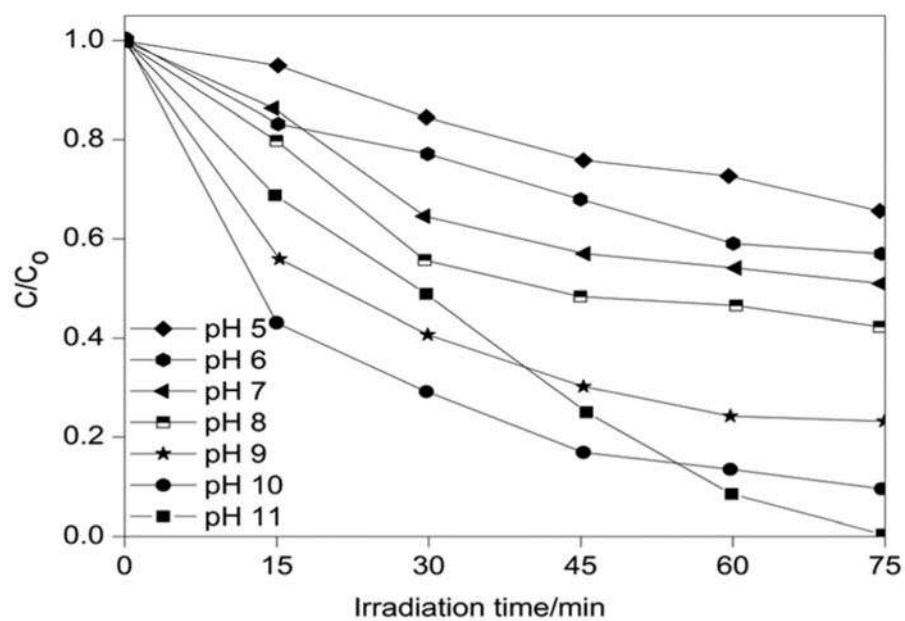


**Fig. 24.** The effect of pH on the photodegradation of MB (catalyst dose = 15 mg; MB concentration =  $1 \times 10^{-6}$  M (= 0.3198 mg L<sup>-1</sup>)).

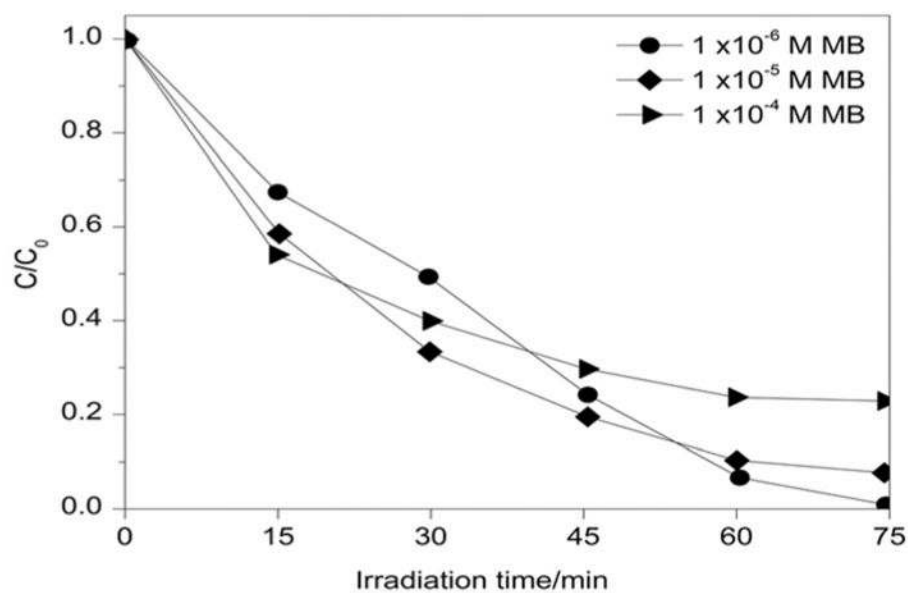


**Fig. 25.** The effect of initial dye concentration on the photodegradation (pH = 11; catalyst dose = 15 mg in 200 ml of MB).

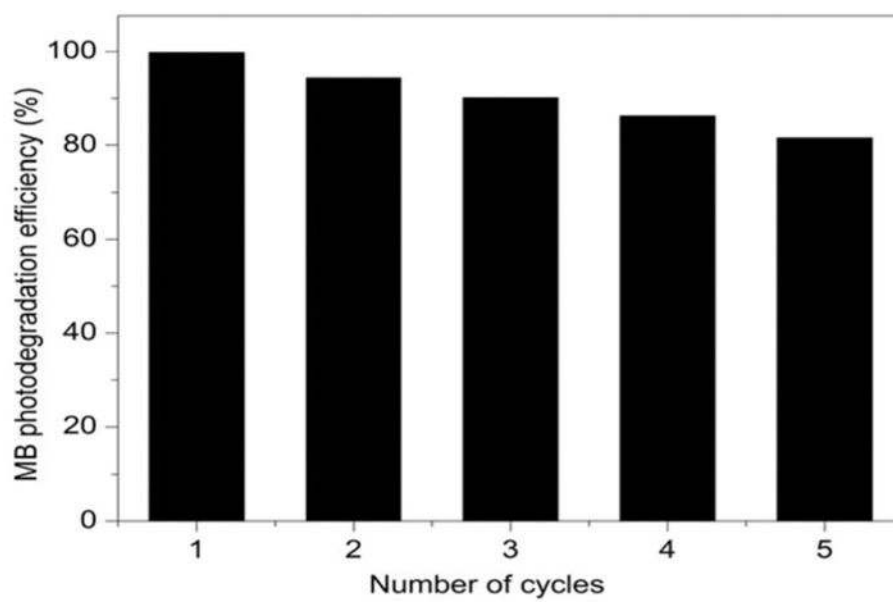


**Fig. 26.** Number of cycles of aqueous MB photodegradation over 2 : 1 Ni/Ti LDH.

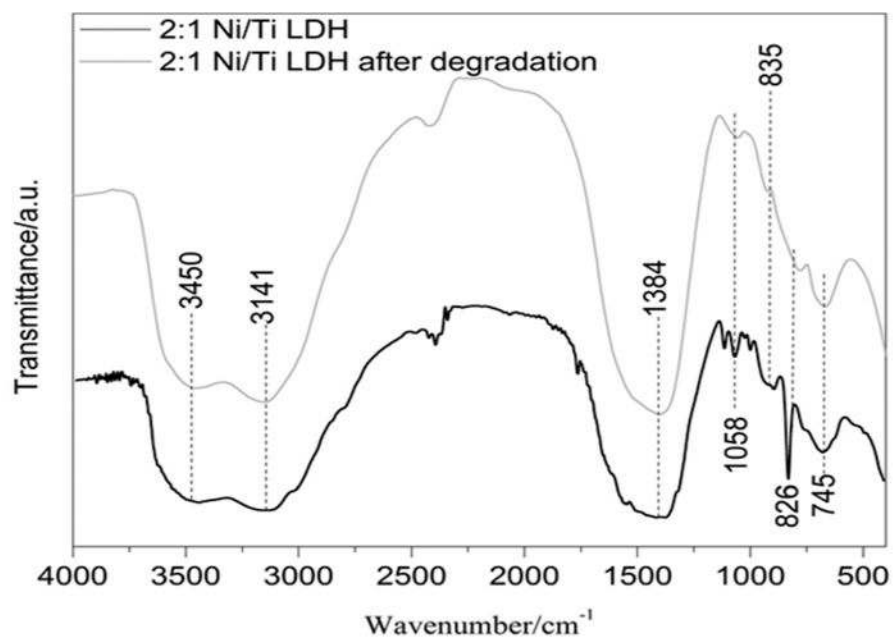
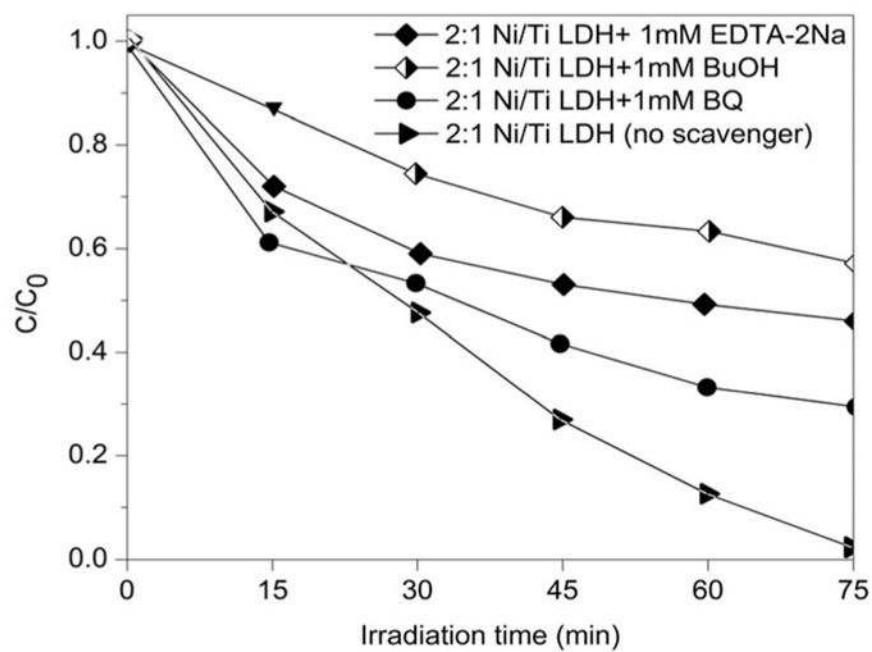
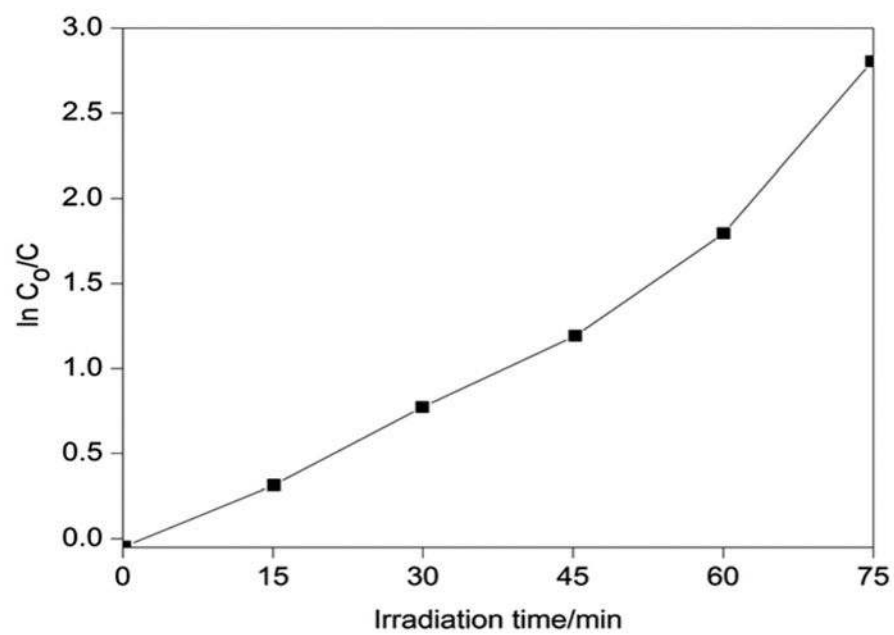


Fig. 27. FT-IR spectra of 2 : 1 Ni/Ti LDH before and after degradation of aqueous MB.



**Fig. 28.** Effects of different active species on the photodegradation of MB (scavenger dosage = 1 mM).



**Fig. 29.** Plot of  $\ln(C_0/C)$  vs. time for 2 : 1 Ni/Ti LDH [pH = 11; catalyst = 15 mg in 200 ml of aqueous MB; MB concentration =  $1 \times 10^{-6}$  M (= 0.3198 mg L<sup>-1</sup>)].

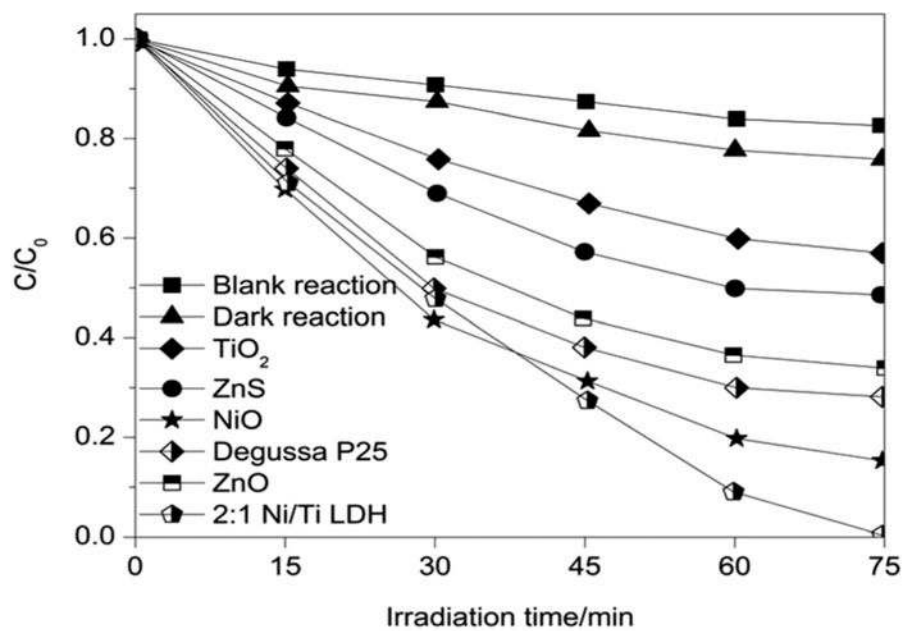


**Fig. 30.** Plot of degradation of aqueous MB ( $C/C_0$ ) as a function of irradiation time for 2 : 1 Ni/Ti LDH with some commercial catalysts.



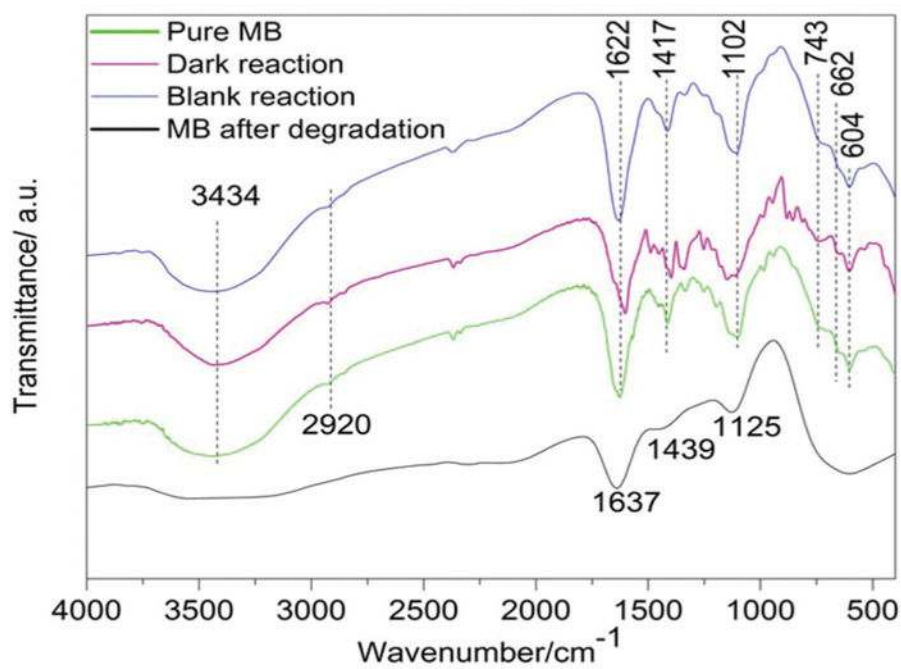


**Fig. 31.**  
FT-IR analysis of the degradation products.

**Table 1**

Elemental composition of EDX analysis for 2 : 1 Ni/Ti LDH

Element	Weight%	Atomic%	Ni/Ti (atomic ratio)
C K	4.45	4.76	2.31
N K	1.47	1.98	
O K	10.13	5.52	
Cl K	3.45	2.75	
Ni K	56.21	59.31	
Ti K	24.29	25.68	
Total	100	100	

Author Manuscript

Author Manuscript

Author Manuscript

Author Manuscript